Characterization of clasts in the Glen Torridon region of Gale crater observed by the Mars Science Laboratory Curiosity Rover

by

Sabrina Y. Khan

Submitted to the Department of Earth, Atmospheric and Planetary Science
in partial fulfillment of the requirements for the degree of

Bachelor of Science in Earth, Atmospheric and Planetary Science

at the

MASSACHUSETTS INSTITUTE OF TECHNOLOGY

May 2021

Author .....
Department of Earth, Atmospheric and Planetary Science
May 14, 2021

Certified by .....
Kristin Bergmann
Professor
Thesis Supervisor

Accepted by .....
Richard Binzel
Chair, Committee on Undergraduate Program

Characterization of clasts in the Glen Torridon region of Gale crater observed by the Mars Science Laboratory Curiosity Rover

by

Sabrina Y. Khan

Submitted to the Department of Earth, Atmospheric and Planetary Science
on May 14, 2021, in partial fulfillment of the
requirements for the degree of
Bachelor of Science in Earth, Atmospheric and Planetary Science

Abstract

Granule- to cobble- sized clasts in the Glen Torridon region of Gale crater on Mars were studied using data captured by the Mars Science Laboratory (MSL) Curiosity rover between martian days ('sols') 2302 and 2593. The morphology and composition of clasts has the potential to reveal the nature and extent of erosional processes acting in a region. In this analysis, measurements of shape, size, texture and element abundance of unconsolidated clasts within lower Glen Torridon were compiled. Eight primary clast types were identified, all of which are sedimentary rock and can be linked to local bedrock, suggesting short transport distances. Several clast types exhibit signs of eolian abrasion, such as facets, pits, flutes and grooves. These results indicate that clasts are the products of bedrock degredation followed by extensive eolian wear.

Thesis Supervisor: Kristin Bergmann
Title: Professor

Acknowledgments

I would like to express my deep gratitude to Professor Kristin Bergmann and Dr. Kathryn Stack, my research supervisors, for their guidance, encouragement and feedback on this research work. I would also like to thank Jane Abbott, for her invaluable advice and assistance in this process.

The work described in this paper was performed at the Jet Propulsion Laboratory, California Institute of Technology, under a contract with the National Aeronautics and Space Administration.

Contents

List of Figures

List of Tables

Chapter 1

Introduction

In-place bedrock geology provides a reliable record of depositional and erosional history, but unconsolidated clasts can also be used to ascertain the dominant modes of modification and transport over local and regional scales. Clasts can log the nature, intensity, and evolution of erosional environments and transport processes they encounter from the time of their formation to the point of deposition within quantifiable parameters such as size, roundness, and circularity. Compositional trends and lithological characteristics can be used as further evidence to tie a clast to its source region. In the case of robotic planetary exploration, clast characterization has the added benefit of aiding and informing rover safety evaluation, as clasts can pose hazards for traversibility. Clasts can also be used as a proxy for bedrock that would otherwise be inaccessible to a rover.

Since landing, the Mars Science Laboratory Curiosity rover has been systematically acquiring images of clasts using the Mastcam and MARDI cameras in the nearfield around the rover at the completion of each of the rover's drives. Syntheses of these clast survey observations in Gale crater were performed at Bradbury Rise and along the traverse to Yellowknife Bay (Yingst et al., 2013, 2016) where unconsolidated clasts were abundant. Building on the work of Yingst et al. (2013, 2016), this study focuses on the characterization of clasts in the Glen Torridon region of Gale crater, where the Curiosity rover encountered an unusually dense collection of granule- to cobble- sized clasts distributed across a region known for its clay-bearing

spectral signatures from orbit (Milliken et al., 2009, 2014; Fraeman et al., 2016) and on the ground (Bristow et al., 2019), and the presence of decameter long-ridges interpreted as periodic bedrock ridges (PBRs) (Stack et al., 2019b). The purpose of this study is to characterize the clasts in Glen Torridon in order to determine their origin, including the mechanisms of formation and modification, and to identify their relationship to the Glen Torridon PBRs.

1.1 Geologic Context

Gale crater is a 155 km diameter impact crater situated along the martian crustal dichotomy boundary, a topographic feature which bisects the heavily cratered southern highlands and the younger northern plains. The crater, which is thought to have formed 3.8-3.6 Ga (Thomson et al., 2011; Deit et al., 2013), contains within it a 5 km thick central mound of sedimentary rock known as Aeolis Mons (informally referred to as Mount Sharp). Gale's extensive record of sustained aqueous activity, particularly the transition from clay-bearing to sulfate-bearing strata observed within the lower reaches of Mount Sharp, motivated its selection as the landing site for the MSL mission (Grotzinger et al., 2014, 2015). Since landing on Bradbury Rise in August 2012, Curiosity has been exploring a thick sedimentary succession of fluvial, fluvial-deltaic, lacustrine and eolian rocks. Beginning around martian day ("sol") 700, Curiosity traversed into the Murray formation, an interval of the Mount Sharp group comprised primarily of finely-laminated mudstones. Murrary formation mudstones have been interpreted to be associated with deposition in a low-energy lacustrine environment that extends nearly continuously from the Pahrump Hills outcrop to this study's region of interest in Glen Torridon (Grotzinger et al., 2015; Fedo et al., 2017; Stack et al., 2019a; Rivera-Hernández et al., 2019; Edgar et al., 2020). During this exploration of the Murray formation, the Curiosity rover has also encountered the Stimson formation of the Siccar Point group, a meter-scale cross-bedded eolian sandstone unit that unconformably overlies the Mt. Sharp group.

Curiosity's exploration of the Glen Torridon region (Fig. 1-1) began on sol 2302

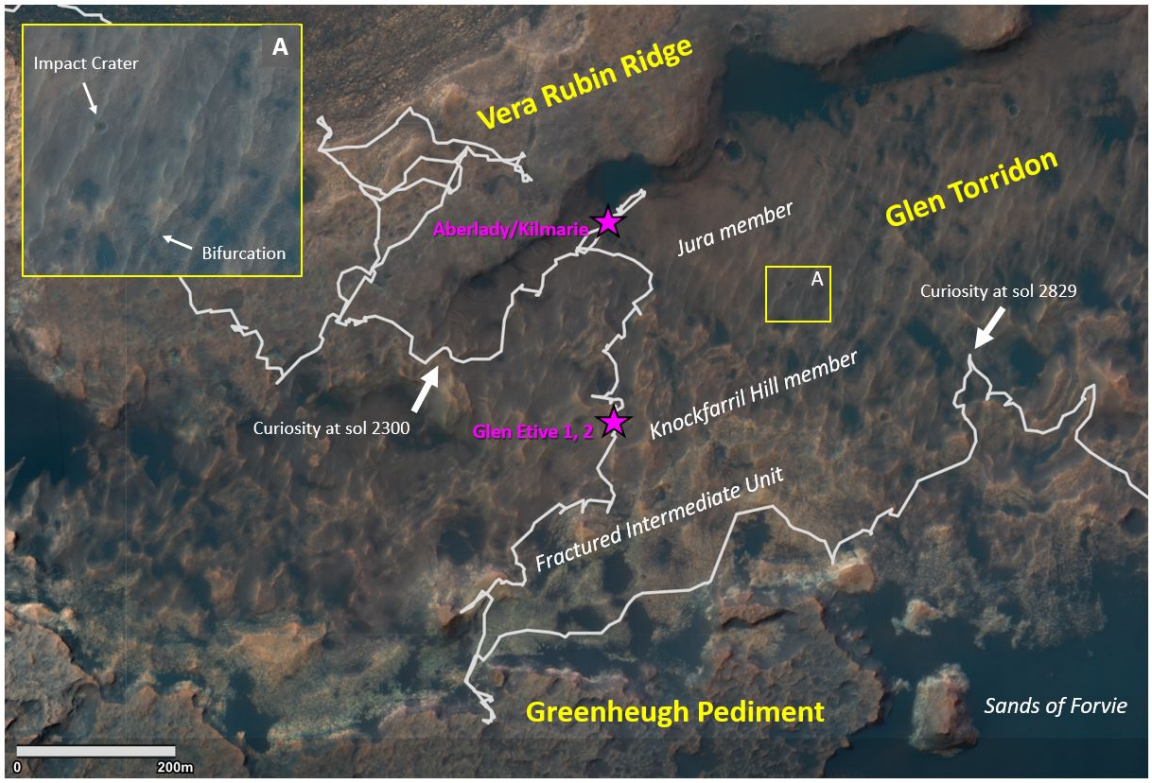

Figure 1-1: Map of the Glen Torridon region within Gale Crater. (A) Eolian ridges interpreted as Periodic Bedrock Ridges (PBRs) (Anderson, 2010; Milliken et al., 2014; Stack et al., 2019b) trending northeast to southwest.

following an ~570 sol campaign at Vera Rubin ridge (VRR) (Fraeman et al., 2020). Orbital observations of this region of Mount Sharp using the High-Resolution Imaging Science Experiment (HiRISE), Context Camera (CTX), Thermal Emission Imaging System (THEMIS), and the Compact Reconnaissance Imaging Spectrometer for Mars (CRISM) revealed a topographic-low with strong phyllosilicate phases and a distinct reticulate texture (Anderson, 2010; Milliken et al., 2009; Fraeman et al., 2016). Compared to the overlying strata which appears to be sulfate-bearing, with little to no apparent clay mineral signatures, Glen Torridon (referred to as "phyllosilicate-bearing trough" in Anderson (2010), "phyllosilicate layers" in Milliken et al. (2010), and "phyllosilicate unit" or "PhU" in Fraeman et al. (2016)), was found to have spectral signatures consistent with Fe/Mg-bearing smectite clays (Fraeman et al., 2016). The transition from clay- to sulfate- bearing units is believed to chronicle a progression of climate change on ancient Mars associated with increasingly arid and acidic

conditions (Milliken et al., 2010; Fraeman et al., 2016; Bibring et al., 2006).

Bedrock exposed within Glen Torridon is interpreted to be stratigraphically equivalent to, and an extension of, the Jura member first identified on VRR (Anderson, 2010; Fraeman et al., 2016). Within Glen Torridon, the Jura member forms a 6 m thick unit of resistant and recessively layered lacustrine mudstone enriched in K and Mg based on ChemCam measurements (Dehouck et al., 2019). A resistant sandstone unit known as the Knockfarril Hill member overlies the Jura member within Glen Torridon (Fox et al., 2020). The Knockfarril Hill member sandstones are easily distinguished by their decimeter-scale cross-bedding and resistance to weathering. The transition between the Jura and Knockfarril Hill members is interpreted to represent a transition from a low- to higher- energy depositional setting (Fox et al., 2020).

One of the most prominent features of Glen Torridon is the presence of decameter-long linear ridges interpreted as periodic bedrock ridges (Stack et al., 2019b), which are prevalent in lower Glen Torridon. Presumed to be transverse to the prevailing wind direction and oriented towards the north-east, the PBRs are interpreted to be carved directly into the bedrock, though they are covered with pebble- to cobble- sized clasts. In this context, understanding the environment in which the Glen Torridon clasts formed may offer insight into the generation of PBRs and the erosion of the Knockfarril Hill member.

Chapter 2

Data and Methods

2.1 Mastcam Clast Survey

Systematic clast imaging has been conducted since Curiosity's landing in Gale crater (Yingst et al., 2010, 2013, 2016). Following nearly every drive completed by Curiosity, a "clast survey" image pair is taken of the ground near the rover with both the left and right eyes of the Mastcam instrument mounted atop the Remote Sensing Mast. The left Mastcam (M-34) has a 34 mm focal length and 18.4° x 15° effective field of view, resulting in a 0.22 mrad/pixel resolution (Malin et al., 2010; III et al., 2013). The right Mastcam (M-100) has a 100 mm focal length, a 6.3° x 5.1° field of view, and a 0.074 mrad/pixel resolution. The standard subframe for clast survey images is 1152 x 1152 pixels, corresponding to a field of view of 14.4°x 14.4° for M-34 and 4.9° x 4.9° for M-100. The image scale is 0.62 mm/pixel and 0.21 mm/pixel for M-34 and M-100, respectively.

Clast survey images are taken at a consistent azimuth (120°) and elevation (-45°) in the coordinate frame of the rover, and most were acquired in the afternoon for consistent illumination in order to provide the best color contrast for distinguishing clasts from the sand substrate (Yingst et al., 2016).

2.2 MARDI

The Mars Descent Imager (MARDI) is a downward-pointing camera intended primarily for navigational use during MSL's entry, descent and landing (Malin et al., 2017). MARDI has since been used to systematically document the terrain covered by Curiosity since its landing in 2012 (Minitti et al., 2019). MARDI has a 70° x 52° field of view and an instantaneous field of view (iFOV) of 76 milliradians, ideal for long-range imaging. MARDI image quality decreases with spatial scale, but post-landing calibration has enabled the instrument to capture 1.5 mm resolution images of the surface directly below the rover (Malin et al., 2009). MARDI's orientation and proximity to the ground (70 mm) offers another dataset uniquely suited to clast imaging. While the resolution of MARDI images is too low to measure physical properties of individual clasts in a reliable and statistically robust way, the images can be used to catalog qualitative morphological features (e.g. texture, angularity, erosional markers), the presence of bedrock, and clast dispersion.

2.3 ChemCam

Elemental geochemistry obtained by the Chemistry and Camera (ChemCam) instrument is assessed in this study to determine compositional trends within clast types and between clast types and local bedrock. ChemCam uses Laser Induced Breakdown Spectroscopy (LIBS) to acquire major element abundances for SiO_2, TiO_2, Al_2O_3, $FeOT$, MgO, CaO, Na_2O and K_2O (Maurice et al., 2012). The LIBS technique involves striking a nearby target with a series of laser pulses to induce a short-lived plasma, from which emitted light produced by atom decay is spectrally analyzed (Maurice et al., 2012). ChemCam is particularly well-suited for clast analysis as it is sometimes able to target multiple small clasts within a single raster and without the need for contact science. In conjunction with LIBS analysis, ChemCam captures sub-millimeter resolution images of targets using its Remote Micro-Imager (RMI). RMI has a field of view of 20 mrad and a pixel scale of 19.6 μrad/pixel (Maurice et al.,

2012). A total of 28 RMI images were used to characterize clast texture and grain size.

2.4 Analysis of Clast Characteristics

Shape and size clast measurements were obtained by analyzing 64 Mastcam clast survey image pairs captured between sols 2302 and 2593. For unbiased clast sampling, 50 x 50 and 10 x 10 grids were superimposed onto the M-34 and M-100 images, respectively. Any clasts within a given cell in the grid were eligible to be sampled and digitally outlined in ImageJ. Following the methods of Yingst et al. (2016), we measured clast major and minor axis, aspect ratio, circularity, solidity, and roundness.

Circularity, C, describes the resemblance of a two-dimensional shape to a circle and is graded on a scale from 0 to 1 (Nurfiani and de Maisonneuve, 2018), going from least to most circular. Circularity is a function of the clast area, A, and clast perimeter, P, given by;

$$C = \frac{4\pi A}{P^2}.$$

Solidity, S, is a measurement of the concavity of a clast, defined as the ratio of clast area, A, to convex hull area, A_c (Nurfiani and de Maisonneuve, 2018). As the clast becomes smoother and more rounded, the area of the clast and that of its convex hull area will converge to 1. Since convex hull area is especially sensitive to surface roughness and protrusions, it has a faster rate of change than the area alone, a trend reflected in the value of solidity.

$$S = A/A_c$$

Roundness is a measure of corner sharpness. Roundness classes defined by Powers (1953) include very-angular, angular, sub-angular, sub-rounded, rounded and well-rounded. Clast roundness is determined by visual assessment.

The accuracy of morphological measurements is highly dependent on image resolution and surface illumination. For the purposes of this study's analysis, the resolution limits on major axis (minimum major axis of 12 mm for M-34 and 4.2 mm for M-100) and shape parameters (minimum major axis of 60 mm for M-34) defined by Yingst et al. (2016) are adopted, with the exception of the minimum major axis limit for shape resolution on M-100 images, which is reduced from 21 mm to 20 mm to incorporate more clasts given the quantity of small pebbles in the region. Any clasts measured below these threshold values were marked and bundled as "fines".

Error in clast morphology measurements is predominantly caused by measurement error and the use of a two-dimensional projection to estimate the parameters of a three-dimensional shape (Yingst et al., 2010), an issue potentially exacerbated by the fact that the fixed orientation of the Mastcam for clast survey images means clasts deposited along slopes are angled differently than those on level ground. Although we acknowledge several potential sources of error, Riley (1941) and Cailleux (1947) show this error to be less than 10% for pebble- to cobble- sized clasts that are sub-angular to well rounded, which is the case for the vast majority of clasts observed in this dataset. We consider this error to be within an acceptable range.

Clast lithology, including texture and grain-size, were assessed qualitatively using Mastcam clast survey images, MARDI images, and finally ChemCam RMI captures where available.

2.5 Approach to Clast and Outcrop Geochemistry

ChemCam targets of in-place bedrock outcrops analyzed between sols 2225 to 2579 were identified as either Jura or Knockfarril Hill member based on their stratigraphic position (elevation) and on a visual assessment of lithology: Jura member is comprised of laminated mudstones; Knockfarril Hill is typically comprised of coarse-grained sandstones. To visualize the major geochemical trends of both members, density contour plots were generated from the bedrock target data. Density contours are two-dimensional histograms used to plot bivariate distributions, which are smoothed

using kernel density estimation for this analysis. The contour lines connect points with the same probability density values and are adjusted according to the number of targets per unit. The major element oxide wt.% is averaged across a target in order to express the effective bulk composition of the target rock.

Clasts compositions were then plotted together with in-situ Jura and Knockfarril Hill member targets in order to compare clast composition with local bedrock. Since rasters tend to span multiple clasts, plots show the composition of individual raster points rather than target averages.

Chapter 3

Results

3.1 Clast types

Based on analysis of shape, size, and texture, eight primary clast types were identified (Fig. 3-1, 3-2). Since features of three-dimensional shapes can be lost in two-dimensional projections, unique and easily distinguishable three-dimensional characteristics such as facets and lineations are recorded by visual assessment. Clast types 1-3 are classified predominantly using such qualitative evaluations. The remaining clast types (4-8) have distinct and quantifiable shape and size characteristics. Individual clasts were sorted into types according to the parameters outlined in Table 3.1.

While all clasts observed are sedimentary, many are coated with a layer of dust which obscures color and grain size, complicating assessments and comparisons of lithology across clast types and bedrock. All but the smallest clasts display some degree of surface polish, but this trait is not unique to any particular clast type. Note that Curiosity generally avoided larger, angular clasts for rover safety, a potential source of bias in this study.

Type 1

These are platy, angular to sub-rounded ($0.17 < R < 0.35$) clasts which often appear lineated. Type 1 clasts tend to be elongate, resulting in high aspect ratios ($1.14 <$

Clast Type	Major Axis (mm)	Solidity	Aspect Ratio	Circularity
Type 1	-	0.77-0.94	> 1.14	-
Type 2	> 10	> 0.90	-	-
Type 3	-	> 0.89	-	-
Type 4	< 5	-	-	-
Type 5	< 18	> 0.94	-	-
Type 6	-	0.83-0.96	> 1.80	< 0.745
Type 7	> 20	> 0.91	> 1.09	> 0.67
Type 8	< 20	> 0.91	> 1.09	> 0.67

Table 3.1: Shape and size parameters of clast types 1-8

AR < 3.7), and have an average clast diameter of 15 mm. Abundance of this clast is low with just over 30 occurrences in the observation period, primarily in the northern region of Glen Torridon. This type occurs commonly on or near bedrock.

Type 2

This type is distinguished by its blocky shape, with multiple flat and smoothed faces oriented at approximately 90°angles from one another. This type is sub-rounded and tends towards high circularity and solidity values. The average diameter of Type 2 clasts is 22.9 mm.

Type 3

Type 3 clasts are sub-rounded and fine-grained down to RMI-scale images. Type 3 clasts contain one or more facets, often marked with grooves, flutes or pits. Unlike the faces of Type 2 clasts, facets tend to meet at obtuse angles and form einkanter or dreikanter shapes after overturning due to excavation of the stoss-side substrate. Many facets exhibit slope retreat towards the apex of the clast, leading some Type 2 clasts to appear curved in plan view. Since Type 2 and 3 clasts cannot be distinguished by shape parameters alone, they are qualitatively sorted in this analysis. Though Type 3 clasts are observable along the full extent of the traverse through Glen Torridon, they are especially common near PBR's and other ridges in the region.

Type 4

This class consists of the smallest observed clasts (d $<$ 4 mm), which are predominantly rounded to well-rounded by qualitative assessment. While these clasts are far below the resolvable size and shape constraints used in this study, these clasts are extremely abundant throughout Glen Torridon.

Type 5

Clasts of this type are rounded to well-rounded with notably high solidity values (S $>$ 0.94), indicating they are relatively spherical with very few protrusions. Texture is smooth and fine-grained. Type 5 clasts are generally small, with diameters less than 18 mm. This type appears in well-sorted patches, especially near topographic lows.

Type 6

This clast is elongated and occasionally has a form reminiscent of a yardang. Type 6 clasts have high aspect ratios (1.8 $<$ AR $<$ 4.6) and low circularity values (C $<$ 0.745). Most clasts of this type are sub-angular to sub-rounded.

Type 7

Type 7 clasts are large pebbles with an average diameter of 25 mm. This type has high solidity (S $>$ 0.91) and an average aspect ratio of 1.4. Nearly all Type 7 clasts have lineations and surfaces which have been smoothed and polished.

Type 8

This class of pebbles have diameters less than 20 mm but are similar in shape to Type 7 clasts. These clasts are abundant throughout Glen Torridon.

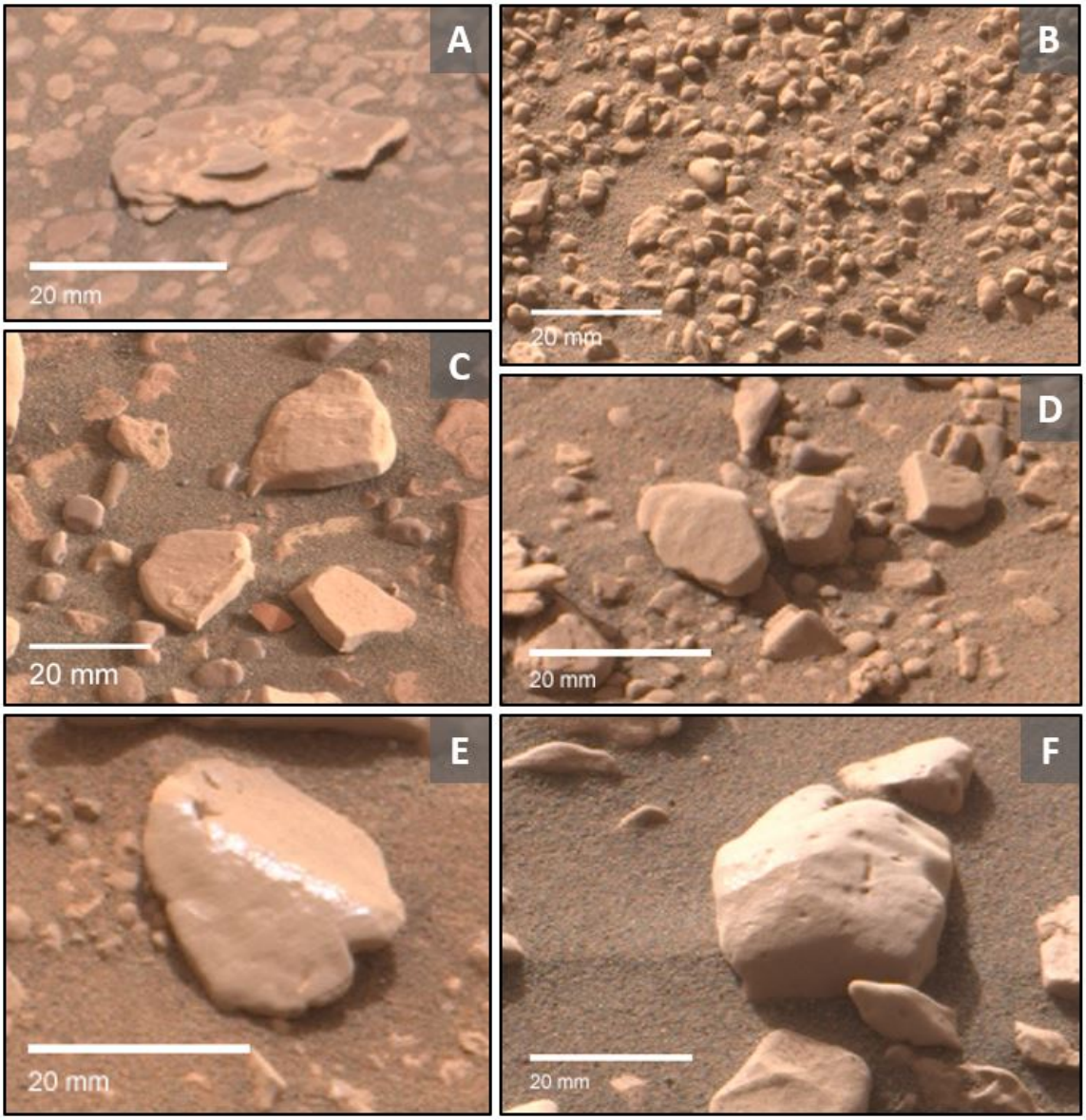

Figure 3-1: M-100 images of clast types 1-4. (A) Type 1 clast, sol 2357, (B) Type 4 clasts, sol 2577, (C) Type 2 clasts, sol 2320, (D) Type 2 clasts which appear to have broken apart in-situ, sol 2480, (E) Type 3 clast, sol 2306, (F) Type 3 clast exhibiting slope retreat towards central keen, sol 2568

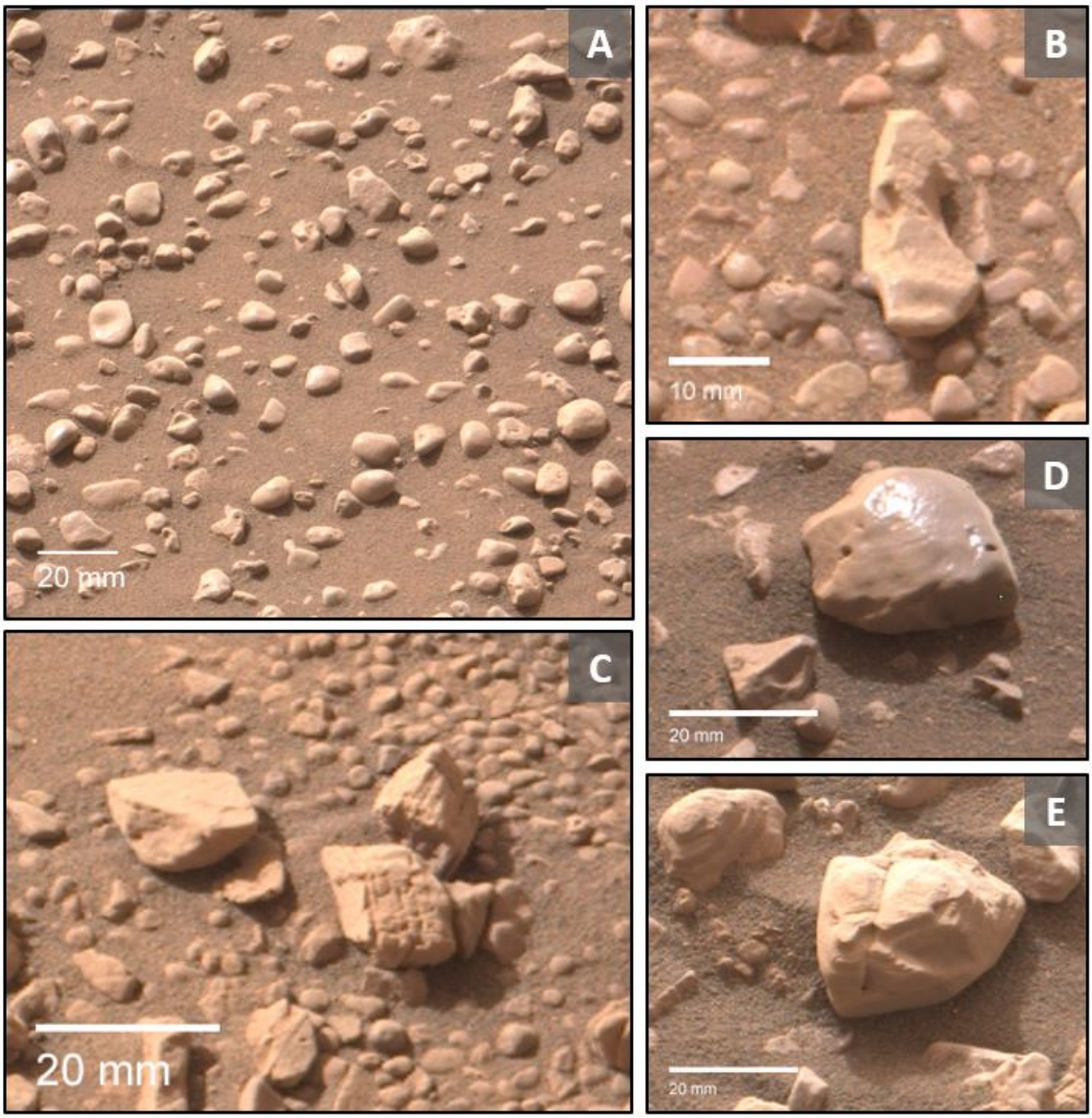

Figure 3-2: M-100 images of clast types 5-8, (A) Type 5 clasts, sol 2466, (B) Type 6 clast, sol 2304, (C) Type 8 clasts, sol 2480, (D) Type 7 clast with polished surface, sol 2477, (E) Type 7 clast with clear lineation, sol 2475

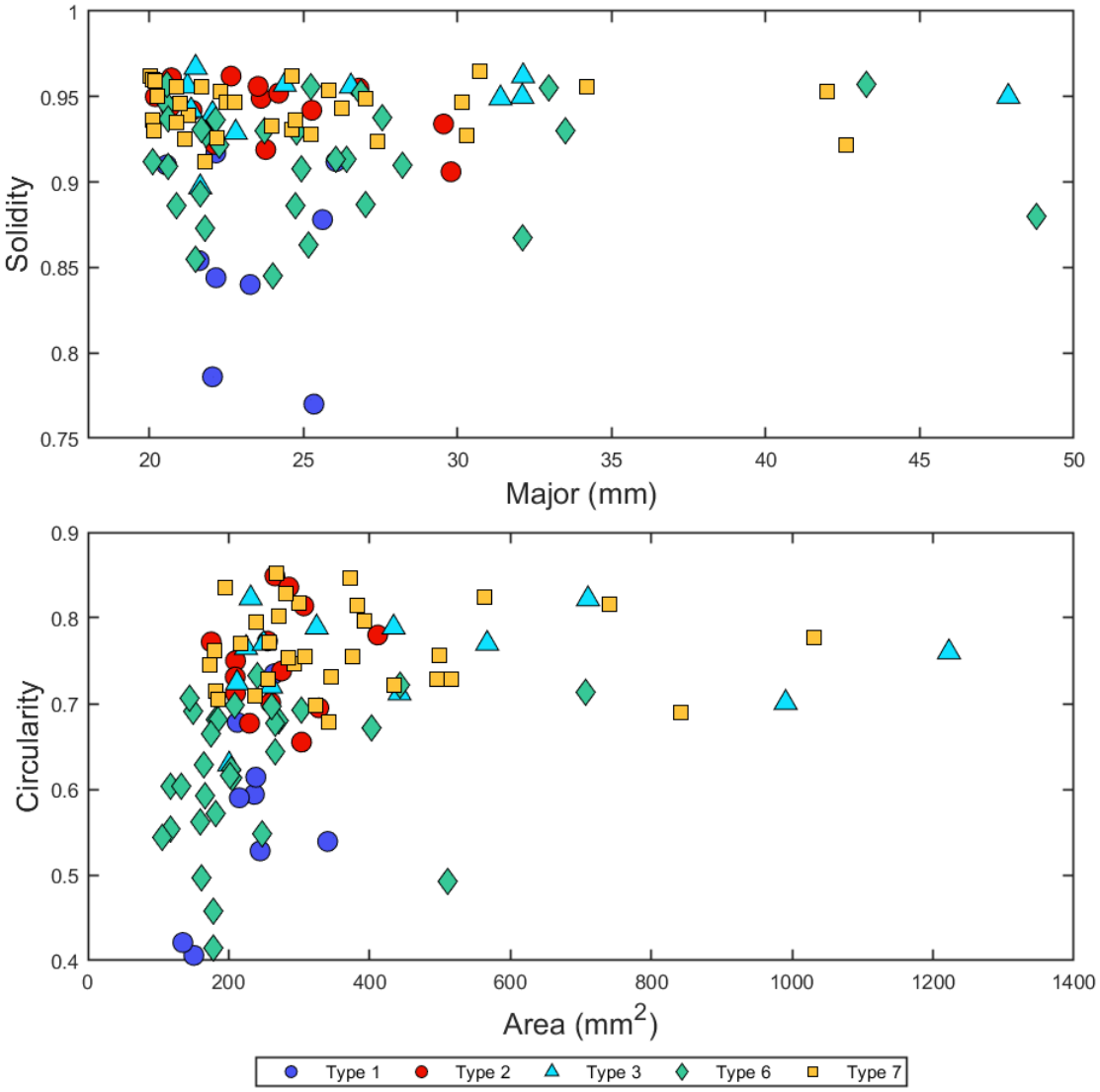

Figure 3-3: Top: plot of clast types as a function of major axis and solidity. Types 1 and 6 largely overlap with the widest range of solidity values. Types 2, 3 and 7 are well constrained to high solidity values but show variability in diameter. Bottom: plot of clast types as a function of area and circularity. Circularity among clasts increases subtly with area. Type 2 clasts are have significantly smaller projected surface areas than Types 3 and 7. Given the shape parameter resolution limit, only clasts with a major axis $>$ 20 mm are plotted, resulting in Types 4, 5 and 8 being excluded.

3.2 Distribution of Clast Types

The spatial distribution of clast types in the Glen Torridon region is mapped in Fig. 3-4. As noted in Section 3.1, Type 1 clasts are predominantly located in northern Glen Torridon. Type 1 clasts rarely coincide with PBRs, possibly because this section of Glen Torridon straddles the base of the southern side of VRR where there are fewer PBRs and a number of dune fields. Type 2 and 3 clasts appear frequently near both smooth and fractured ridges, including those oriented discordant to the northeast to southwest bearing of the local PBRs.

Type 7 clasts are infrequent, but scattered almost uniformly along Curiosity's traverse. They appear to be densely packed near ridges. By contrast, the remaining clast types (4, 5, 6, 8) are abundant with no apparent bias towards any locality of Glen Torridon or any of its geologic features.

3.3 Proximity to Periodic Bedrock Ridges

Four PBRs were identified along the rover traverse with more than one Mastcam clast survey image taken within 15m of the PBR crest (Fig. 3-6). Trends in shape and size parameters with respect to distance from the PBR crest are illustrated in Figure 3-6. PBR 2 displays a drastic change in all measured parameters near the crest, which can be explained by the PBR's proximity to a large Knockfarril Hill member outcrop within several meters of where the Mastcam clast survey image was taken on that sol. The remaining PBRs reflect similar patterns. In general, aspect ratio is shown to decrease downslope, while circularity and area increase. Trends in solidity and major axis are less consistent.

3.4 Geochemistry

Major element abundances measured by the ChemCam instrument show clast composition is closely correlated with bedrock composition (Fig. 3-5), consistent with the findings of Dehouck et al. (2019). Over 63% of the raster points representing

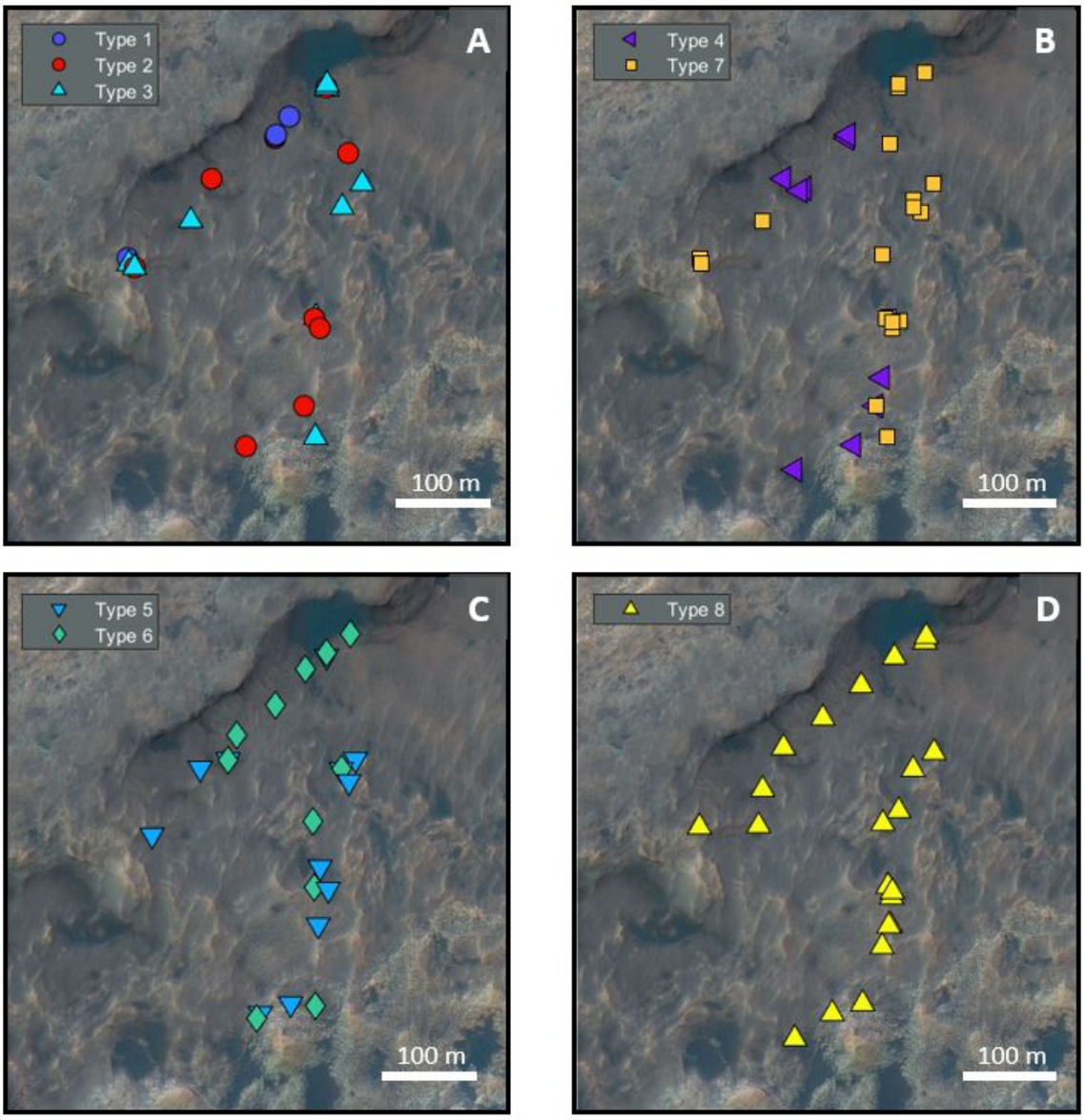

Figure 3-4: Spatial distribution of clast types. Points in (A) and (B) represent locations where clast types represent ≥5% of the sampled population, since these types occur infrequently. Points in (C) and (D) represent locations where clast types represent ≥30% of the sampled population. Type 4 clasts are mostly under the major axis resolution limit and thus appear localized, but in fact these clasts are abundant along the traverse

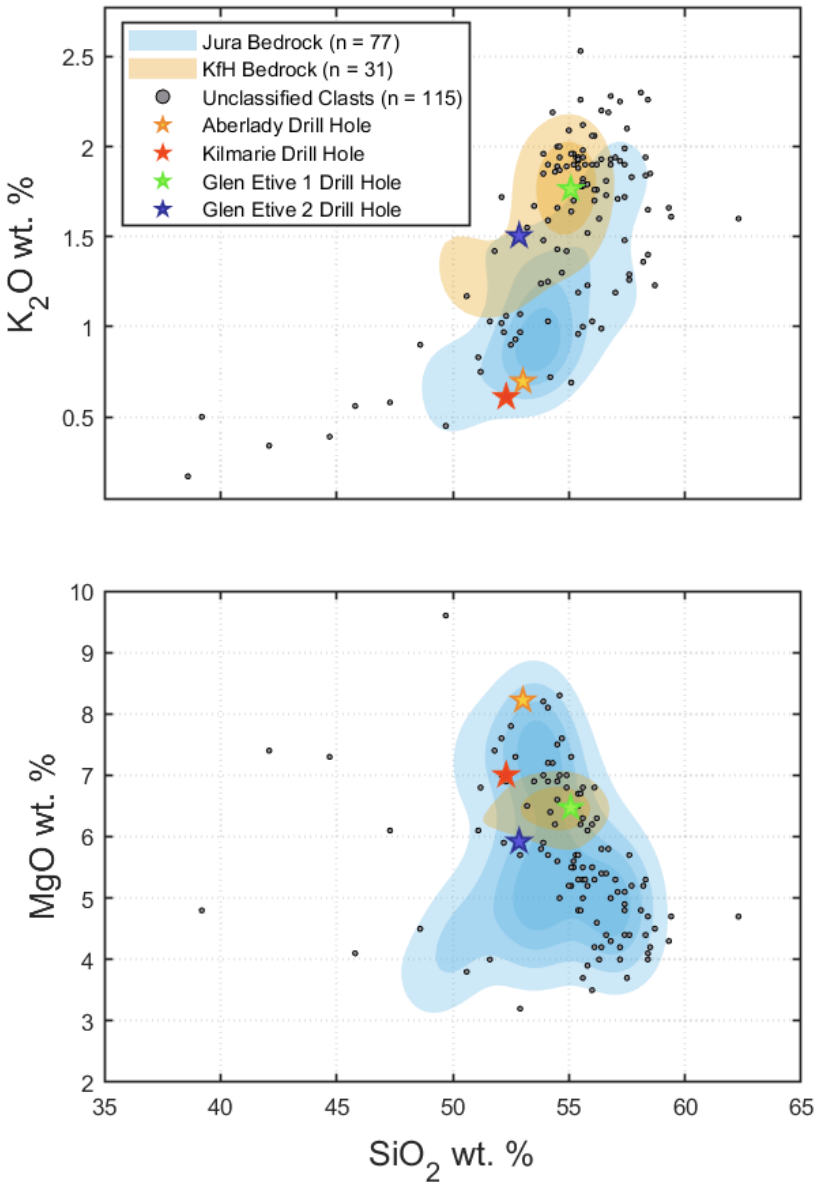

Figure 3-5: Density contours of Jura and Knockfarril Hill members for select major element oxides, averaged by target. The Knockfarril Hill contour is elevated in K_2O and depleted in MgO compared to Jura. The average compositions of drill targets, represented by stars, reflect this trend. Aberlady and Kilmarie samples were taken from Jura bedrock, while Glen Etive samples 1 and 2 are taken from Knockfarril Hill.

unclassified clasts are enriched in K_2O (> 1.5 wt. %), suggesting a majority of clasts in Glen Torridon are sourced from the Knockfarril Hill member. However, a large portion of the clasts also display enrichment in MgO, a trait of the Jura member, indicating the provenance of the clasts analyzed in this study is primarily within Glen Torridon itself.

While the geochemistry dataset does not correspond to the Mastcam or MARDI clast imagery, the drill targets (Aberlady, Kilmarie, Glen Etive 1, Glen Etive 2) are useful for understanding which clast types are associated with the Jura and Knockfarril Hill units. Aberlady and Kilmarie are drill holes on the same bedrock outcrop within the Jura member. Clasts near this bedrock outrcrop vary widely in size, but are predominantly flat and wide or blocky and sub-rounded in shape, corresponding to Type 1 and 2 clasts. Since Type 1 clasts are local to northern Glen Torridon, this type could be interpreted as predominantly Jura member with a high MgO signature.

In the immediate vicinity of the Knockfarril Hill targets, Glen Etive 1 and Glen Etive 2, are well-rounded granules and pebbles embedded in the sand, overlain by larger sub-angular to sub-rounded clasts. The appearance of these clasts is broadly consistent with the definitions of clast types 4 and 5, and 2 and 8, respectively. All of these types are known to be abundant throughout Glen Torridon, and thus cannot be confidently tied to a particular member or compositional signature.

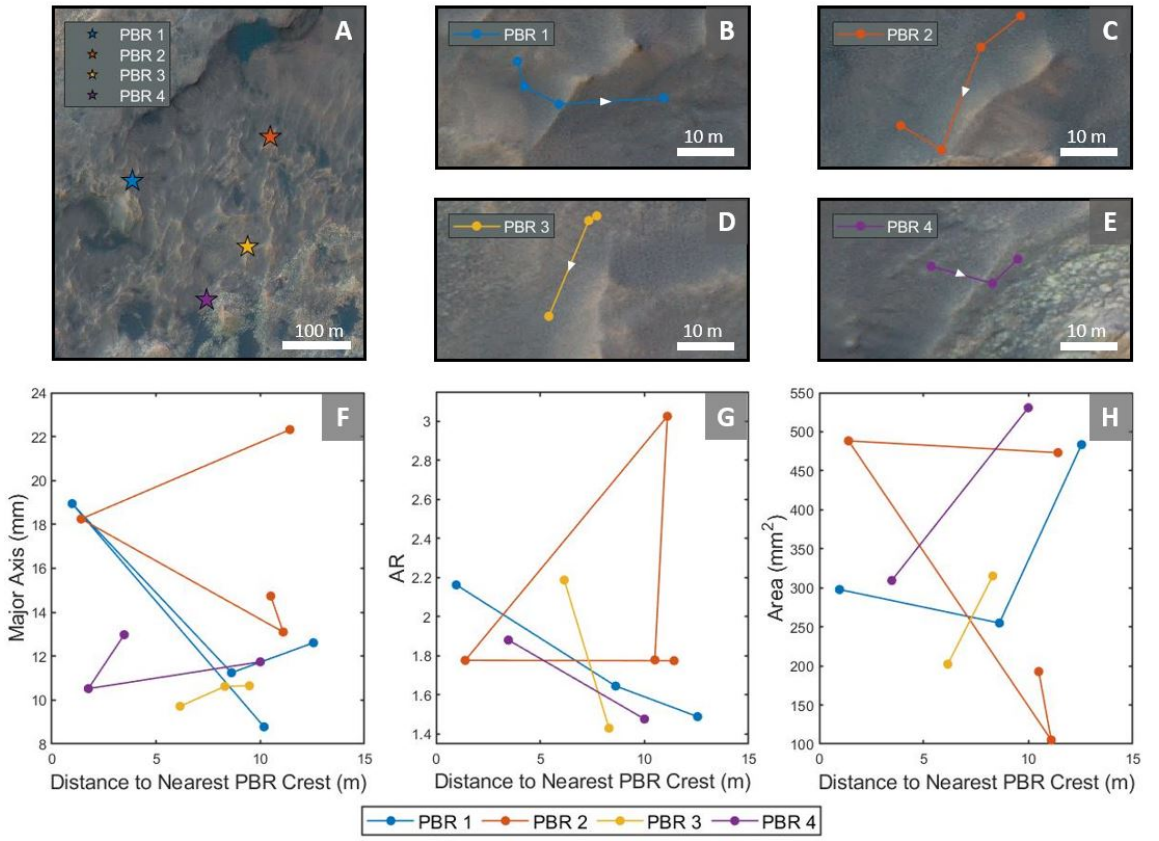

Figure 3-6: (A) Map of PBR locations in Glen Torridon along the Curiosity traverse. (B)-(E) Represents rover positions with respect to each PBR. The direction of rover travel is indicated by the white arrow. (F)-(H) The averaged morphologies of clasts imaged at each rover position along the PBR are presented with respect to approximate distance from the PBR crest. The connecting lines indicate the direction of rover travel towards or away from the crest in accordance with maps B-E.

Chapter 4

Discussion

4.1 Process of clast formation and modification

We propose four possible processes by which the clasts observed may have been formed and modified: (1) mega-ripple detachment from PBRs, (2) impact cratering, (3) fluvial or debris flow, and (4) in-situ bedrock degradation.

Mega-ripple detachment

The existing hypothesis for PBR formation offered by Hugenholtz et al. (2015) is tied to mega-ripple development on friable bedrock. Clasts shed from the bedrock layer are driven by wind-processes to produce mega-ripple crests, which in turn shield the underlying bedrock from further erosion. In the intermediate zones with minimal clast cover, erosion carves troughs directly into the bedrock. The mega-ripples (unconsolidated clasts) remain attached to the crest of the newly formed PBR until they eventually detach and slide down the lee side of the ridge. In this model, the Glen Torridon clasts are remnants of detached mega-ripples which have undergone extensive eolian abrasion after settling into the troughs of PBRs. This mechanism could explain the abundance of clasts in Glen Torridon and is supported by the presence of small eolian bedforms encountered along the traverse, but stands in contrast to the experimental findings of Hugenholtz et al. (2015) which show the mega-ripple clasts evacuating the field of PBRs altogether and exposing the crests to scalloping

as a result. It is possible that the thin atmosphere on Mars prevents entrainment of granule- to cobble- sized clasts by the wind, preventing the clasts from leaving the topographic low formed by the PBR crests. The enhanced abrasion experienced by clasts confined to troughs support observations of small rounded to well-rounded (Type 4, Type 5) clasts at these locations as well.

Impact cratering

Craters disrupt bedrock ridges in multiple locations across Glen Torridon (Fig. 1-1A), presenting another possible source of granules, pebbles and cobbles. Impact ejecta is largely angular with variable sphericity (Yingst et al., 2016) and could explain the unusually jagged appearance of Type 1 clasts. Even so, a majority of the clasts in the region are sub-angular to rounded. Taking into account the sheer abundance of clasts in the region, it is unlikely that impacts alone are the dominant process for clast formation. However, highly angular cobble-sized clasts with no apparent relation to local deposits, notable especially in the PBR troughs where clasts are are occasionally well-sorted in size and shape, may be linked to impact events.

Fluvial or debris flow

In the case of a fluvial or debris flow event, large quantities of clasts could be transported from flows travelling either down Mount Sharp or the nearby Vera Rubin Ridge (VRR). Debris flows are easily able to transport granule- to cobble- sized clasts (Whipple and Dunne, 1992), and studies of the Peace Vallis alluvial fan at the crater rim indicate fluvial flows can support clasts up to 10 cm in diameter (Sautter et al., 2014, 2015; Cousin et al., 2021). This model could reasonably explain the abundance of clasts and the prevalence of rounded Type 4 and 5 varieties irrespective of local geologic features such as PBRs and other ridges. Additionally, abrasion in fluvial flows is able to produce features typically associated with ventifacts (wind formed clasts; pits, grooves, flutes, and facets) (Durand and Bourquin, 2013) which are common in Type 3 clasts. Facets developed in fluvial conditions tend to be rougher than those generated by eolian abrasion, but subsequent modification by wind processes could

eventually smooth and polish these surfaces. Angular deposits can be accounted for in this model by shorter transport distances.

Both transport mechanisms would likely entrain sediments from the upper slopes of Mount Sharp or VRR, leading to some lithological and geochemical diversity. As described in Section 3.4, nearly all clasts analyzed in this study using ChemCam are interpreted as Jura or Knockfarril Hill member. The fractured intermediate unit (fIU) and Greenheugh pediment south of Glen Torridon towards Mount Sharp (Fig. 1-1) are distinct both lithologically and in composition (Bryk et al., 2020). The fIU in particular is depleted in K_2O and MgO compared to the mean Jura and Knockfarril Hill member compositions (O'Connell-Cooper et al., 2021). It is unlikely Glen Torridon clasts are sourced from either of these units.

While Jura member on Vera Rubin ridge does have lithological similarities to Jura in Glen Torridon, there exists significant differences in composition, namely in Fe, Ti, Cr, Cr, S, Al, Na, Ca and Ni abundances according to Alpha Particle X-Ray Spectrometer (APXS) measurements (O'Connell-Cooper et al., 2021). Unfortunately APXS data is not readily available for clasts as APXS is a contact-science instrument, making it difficult to verify whether VRR Jura is present in Glen Torridon. Even so, only about 30% of Glen Torridon clasts are interpreted as Jura member. Fluvial and debris flows from VRR would not account for the majority of pebbles observed in the region.

In-situ bedrock degradation

Another pathway capable of producing the quantity of clasts in Glen Torridon is through the degradation of bedrock into cobbles, pebbles and granules. In this scenario, clasts detach from bedrock along pre-existing fractures and bedding planes. Gravity and wind-action transport clasts into topographic lows, where they are exposed to enhanced eolian abrasion. Bedrock degradation is expected to preferentially decay the overlying Knockfarril Hill member until Jura member bedrock is exposed.

The Jura and Knockfarril Hill members of Glen Torridon both display a tendency to fracture in accordance with this model. The Woodland Bay outcrop of the Jura

member has interbedded thick and thin layers (Fig. 4-1) separated by fracture fill material. Clasts in the immediate vicinity of Woodland Bay, identified as Type 2 clasts, exhibit similar morphologies as the blocks that make up bedding layers of this outcrop. Similarly, outcrops of the Knockfarril Hill member are bedded and appear to fracture along fracture fills as well as internally. Near the Risk target in the Knockfarril Hill member are clasts which appear to have recently detached from the bedrock, including blocky Type 2 clasts, and angular clasts reminiscent of Type 7 and 8 clasts which may have formed as the result of internal fracturing.

The presence of smectite clay-minerals in Glen Torridon may contribute to the friability of both members. Smectite clays are a type of phylosillicate clay susceptible to swelling when exposed to water. The smectites are composed of alternating layers of tetrahedral silicate and octahedral Al, Fe or Mg sheets (Fraeman et al., 2016). Cations in the interlayers readily absorb water, causing the clay to expand in proportion to the water available. Hydrated smectites shrink and crack upon drying. Previous studies interpret the transition from clay-bearing to sulfate-bearing units from Glen Torridon to the nearby fractured intermediate unit (fIU) to represent the shift from a wet environment to the dry and arid climate of Mars today (Milliken et al., 2010). Such a transition could induce the shrinking of hydrated smectites in Glen Torridon, leaving the Jura and Knocfarrill Hill members cracked and vulnerable to further breakage.

4.2 Interpretation of Glen Torridon clasts

The friable and rubbly nature of both Jura and Knockfarril Hill member bedrock points to in-situ bedrock degradation as the most likely case for clast formation in Glen Torridon. Outcrops such as Woodland Bay, North Berwick and the Glen Etive drill site provide ample evidence of clasts in the process of loosening from the bedrock along fracture fills, laminations and recessive bands. Clasts near bedrock outcrops are generally more angular, blocky or platy, while lacking prominent surface features like pits, flutes and facets, a strong sign of recent erosion.

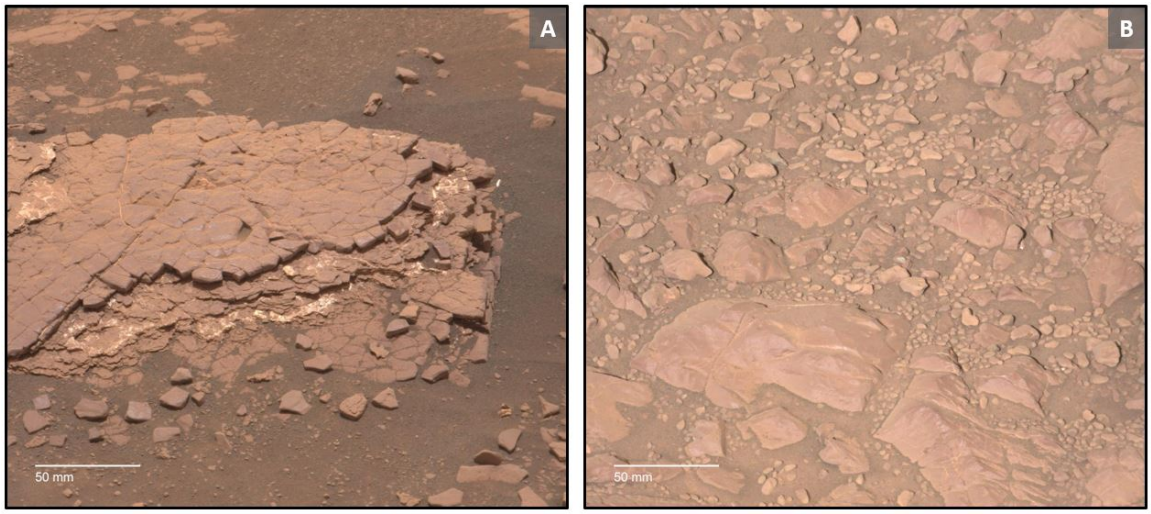

Figure 4-1: (A) Woodland Bay outrcrop, sol 2359 of the Knockfarril Hill member within Glen Torridon. (B) Arnaboll outcrop, sol 1957, of the Jura member on Vera Rubin Ridge

Unlike the fluvial, debris flow and impact cratering models, bedrock degradation explains the proportion of Jura to Knockfarril Hill member clasts described in Section 3.4. The overlying Knockfarril Hill member is exposed to erosion before Jura, allowing descendant clasts to accumulate in the region. The mega-ripple detachment hypothesis would produce a similar fractionation, but this formation pathway links PBR development to clast formation. Since clasts are especially abundant in the fractured ridge unit of Glen Torridon where PBRs are uncommon, it is unlikely that this mechanism produces clasts.

Figure 4-2 illustrates the proposed lifecycle of clasts in Glen Torridon after eroding from bedrock. Given their frequent appearance near bedrock, angularity and shape reminiscent of cracked bedding layers, Type 1 and Type 2 clasts are suspected to be the most freshly loosened clasts. Type 1's form from multiple thin bedding layers sloughing off in unison, while Type 2's are the result of a single thick bedding layer detaching into multiple blocky units (e.g. Woodland Bay, Fig. 4-1). Attempts to drill into the Jura member at the Aberlady drill site resulted in the uplift of a bedding layer which had a similar morphology as many of the Type 1 clasts observed in this study.

Type 7 clasts are also interpreted as recently eroded clasts on account of their

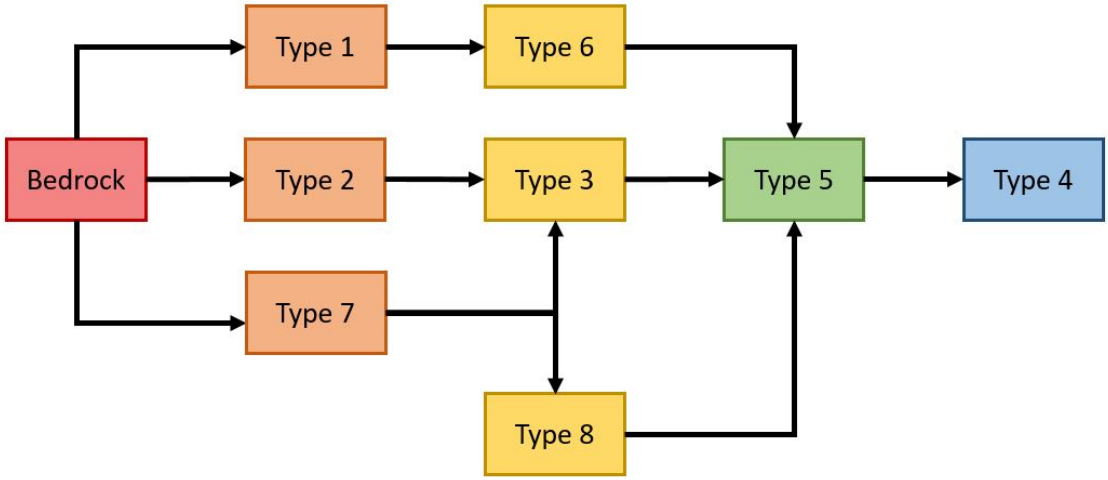

Figure 4-2: Proposed clast lifecycle. Rounding, solidity and circularity increase from left to right.

size. The average clast diameter in Glen Torridon is 12 mm, while the average Type 7 clast diameter is closer to 25 mm. Though Type 7 clasts appear throughout the traverse (see Fig. 3-4), they are noticeably more common near large outcrops of the Knockfarril Hill member and PBR formations. Whether their formation is tied to either one of these features is unclear.

After shedding, the clasts become exposed to eolian abrasion. Type 1 clasts appear to weather into Type 6 clasts, which have similarly high aspect ratios and low solidity values. Type 2 and Type 7 clasts appear to evolve into Type 3 clasts, developing facets and other signs of eolian wear. All three clast varieties have similar shape characteristics. Importantly, Type 3 clasts have an average area between Types 2 and 7, suggesting lineage from both types. The relatively smooth texture and polished surfaces of most Type 3 clasts also indicate the clasts are in an intermediate stage of development. Wind-tunnel tests conducted by Bridges et al. (2004) in martian atmospheric conditions found ventifacts grow rougher, not smoother, with time. Similarly, Bridges et al. (2004) determined that ventifact development is a function of initial shape, with steeper faces relative to wind direction forming pits and shallow faces forming grooves. The existence of both features on Type 3 clasts supports the conclusion that they are derived from blocky Type 2 clasts.

Type 2 and Type 7 clasts seemingly also erode into Type 8 clasts, which are smaller and vary in roundness. This may result from enhanced eolian abrasion, or further fracture of the clast (as seen at the Risk target within the Knockfarril Hill member).

Over time, all clasts are expected to erode into Type 5 and Type 4 clasts, which are smaller, more rounded, and far more abundant than any other clast type.

4.3 Relationship to PBRs

Since clasts are observed in areas where PBRs are uncommon, PBRs are not interpreted as a necessary precursor to or consequence of unconsolidated clasts. However, exposed bedrock at ridge crests is a potential source for new clast formation, which could explain the abundance of Type 2 and Type 7 floats in close proximity to their slopes.

The trends observed in Section 3.3 may be interpreted in one of two ways: either (1) clasts become rounded as they are transported down the ridge face, with larger clasts preferentially being transported into the troughs on account of their size, or (2) smaller, angular clasts form near the PBR crest while larger, rounder clasts form independently at the troughs.

Given the heightened erosion at PBR crests, it is likely wind is responsible for loosening large clasts which are then transported downslope, causing accumulations of Type 2 and 7 clasts in the troughs, while smaller clasts remain on the slopes or near the peaks. Any large enough clasts on the slope or near the base of the PBR developed into Type 3 clasts as a result of wind-driven saltating sand grains.

Smaller clasts in the presence of wind were likely overturned and redistributed (Pelletier et al., 2009), rounding the clast with time and perhaps driving the formation of smaller eolian bedforms throughout the region.

Chapter 5

Conclusion

Clast morphology and surface features enabled sorting of clasts within Glen Torridon into eight characteristic types. The spatial distribution of these types indicates the formation of Type 1 clasts is associated with the Jura member, while Type 2 and 3 clasts are associated with periodic bedrock ridges. The reflection of high Mg and high K signatures typical of Jura and Knockfarril Hill members, respectively, in clasts sampled throughout Glen Torridon indicate that the clasts are formed in the region. Taking the results of clast morphology, spatial distribution and geochemistry data together, we propose that clasts within Glen Torridon are the result of in-situ bedrock degredation facilitated by eolian abrasion. Enhanced and directional winds in the troughs and on the slopes of PBRs serve to drive clast smoothing, rounding and mass loss over long timescales.

Future studies may incorporate clast morphology and distribution analysis to determine clast erosion rates, which may help constrain paleowind speeds and directions. Results of such studies may be used to further our understanding of the formation and modication of the periodic bedrock ridges characteristic of the Glen Torridon region.

Appendix A

Clast Measurements

CLAST ID	SOL	AREA (MM^2)	MAJOR (MM)	CIRC.	AR	SOLIDITY	LATITUDE (°)	LONGITUDE (°)	ELEVATION (M)
1	2302	796.402	33.345	0.626	1.097	0.96	-4.72915	137.38	-4141.97
6	2302	841.031	42.621	0.689	1.696	0.922	-4.72915	137.38	-4141.97
10	2302	300.012	22.301	0.817	1.302	0.953	-4.72915	137.38	-4141.97
21	2302	212.121	20.553	0.678	1.564	0.91	-4.72915	137.38	-4141.97
27	2302	267.687	24.608	0.664	1.777	0.922	-4.72915	137.38	-4141.97
10	2304	272.803	21.445	0.615	1.324	0.884	-4.72925	137.38	-4141.65
11	2304	205.594	24.748	0.613	2.34	0.886	-4.72925	137.38	-4141.65
19	2304	211.856	21.231	0.724	1.671	0.956	-4.72925	137.38	-4141.65
29	2304	346.053	25.248	0.731	1.447	0.928	-4.72925	137.38	-4141.65
31	2304	238.493	20.887	0.795	1.437	0.956	-4.72925	137.38	-4141.65
1	2306	327.972	29.542	0.695	2.09	0.934	-4.72932	137.3801	-4141.14
5	2306	324.841	24.392	0.789	1.439	0.957	-4.72932	137.3801	-4141.14
9	2306	510.237	48.797	0.492	3.665	0.88	-4.72932	137.3801	-4141.14
10	2306	434.164	26.536	0.789	1.274	0.956	-4.72932	137.3801	-4141.14
15	2306	260.234	22.8	0.72	1.569	0.929	-4.72932	137.3801	-4141.14
16	2306	164.14	21.856	0.629	2.286	0.928	-4.72932	137.3801	-4141.14
17	2306	182.045	20.113	0.714	1.745	0.936	-4.72932	137.3801	-4141.14
19	2306	403.03	33.497	0.672	2.187	0.93	-4.72932	137.3801	-4141.14
20	2306	162.112	27.008	0.496	3.534	0.887	-4.72932	137.3801	-4141.14
25	2306	209.74	22.123	0.712	1.833	0.922	-4.72932	137.3801	-4141.14
7	2313	235.362	30.886	0.491	3.183	0.804	-4.72847	137.3812	-4147.44
18	2313	392.446	27.009	0.796	1.46	0.949	-4.72847	137.3812	-4147.44
24	2313	253.046	21.936	0.687	1.494	0.891	-4.72847	137.3812	-4147.44
27	2313	195.892	20.031	0.835	1.609	0.962	-4.72847	137.3812	-4147.44
25	2316	267.202	20.09	0.852	1.186	0.96	-4.72809	137.3813	-4148.29
28	2316	116.821	20.579	0.603	2.847	0.945	-4.72809	137.3813	-4148.29
2	2320	254.986	23.623	0.773	1.719	0.949	-4.72772	137.3815	-4150.33
8	2320	265.526	20.712	0.849	1.269	0.961	-4.72772	137.3815	-4150.33
11	2320	411.541	26.797	0.78	1.37	0.955	-4.72772	137.3815	-4150.33
12	2320	209.695	20.668	0.75	1.6	0.944	-4.72772	137.3815	-4150.33
9	2350	292.471	22.207	0.746	1.324	0.926	-4.72794	137.3818	-4150.45
4	2354	191.218	27.629	0.485	3.135	0.816	-4.72719	137.3823	-4152.26
7	2354	117.306	21.495	0.554	3.093	0.855	-4.72719	137.3823	-4152.26
12	2354	177.811	32.114	0.414	4.555	0.867	-4.72719	137.3823	-4152.26
2	2359	208.814	22.166	0.698	1.848	0.936	-4.7266	137.383	-4155.24
6	2359	203.786	21.65	0.623	1.806	0.893	-4.7266	137.383	-4155.24
1	2365	566.994	32.1	0.77	1.427	0.95	-4.72608	137.3837	-4157.94
3	2365	175.165	20.189	0.772	1.828	0.95	-4.72608	137.3837	-4157.94
12	2365	284.71	21.281	0.754	1.249	0.939	-4.72608	137.3837	-4157.94
15	2365	182.001	25.157	0.571	2.731	0.863	-4.72608	137.3837	-4157.94
3	2407	376.57	23.948	0.755	1.196	0.933	-4.72602	137.3837	-4158.09
6	2407	224.557	21.35	0.765	1.594	0.942	-4.72602	137.3837	-4158.09
2	2413	516.058	30.292	0.729	1.397	0.927	-4.72582	137.3841	-4157.71

4	2416	302.791	27.54	0.693	1.967	0.938	-4.72631	137.3833	-4156.98
1	2420	150.469	22.046	0.406	2.537	0.786	-4.72696	137.3827	-4153.94
2	2420	134.858	25.336	0.421	3.739	0.77	-4.72696	137.3827	-4153.94
3	2420	244.623	22.156	0.528	1.576	0.844	-4.72696	137.3827	-4153.94
4	2420	236.42	26.051	0.594	2.254	0.912	-4.72696	137.3827	-4153.94
23	2420	264.953	22.154	0.735	1.455	0.917	-4.72696	137.3827	-4153.94
8	2422	215.12	25.617	0.59	2.396	0.878	-4.72693	137.3827	-4154.07
13	2422	238.493	21.61	0.614	1.538	0.854	-4.72693	137.3827	-4154.07
26	2422	340.452	23.268	0.539	1.249	0.84	-4.72693	137.3827	-4154.07
27	2422	240.566	20.372	0.678	1.355	0.905	-4.72693	137.3827	-4154.07
1	2429	312.052	26.591	0.711	1.78	0.91	-4.72709	137.3835	-4154.08
11	2429	246.784	23.997	0.548	1.833	0.845	-4.72709	137.3835	-4154.08
18	2429	434.165	24.611	0.721	1.096	0.931	-4.72709	137.3835	-4154.08
4	2432	259.617	25.267	0.701	1.931	0.942	-4.72726	137.3841	-4152.44
14	2432	220.5	27.743	0.539	2.741	0.824	-4.72726	137.3841	-4152.44
6	2434	184.823	20.124	0.705	1.721	0.93	-4.72781	137.3843	-4150
14	2434	200.655	21.647	0.629	1.834	0.897	-4.72781	137.3843	-4150
5	2435	105.09	20.123	0.544	3.026	0.912	-4.72793	137.3842	-4145.68
6	2436	323.297	26.247	0.698	1.674	0.943	-4.72811	137.3839	-4148.49
8	2436	180.986	20.594	0.681	1.84	0.909	-4.72811	137.3839	-4148.49
6	2439	705.997	43.271	0.713	2.083	0.957	-4.72833	137.3841	-4144.81
7	2439	270.642	22.495	0.802	1.468	0.947	-4.72833	137.3841	-4144.81
1	2447	990.707	50.356	0.701	2.01	0.953	-4.72824	137.3839	-4147.06
2	2447	249.65	22.046	0.77	1.529	0.94	-4.72824	137.3839	-4147.06
7	2447	179.178	20.164	0.762	1.782	0.959	-4.72824	137.3839	-4147.06
2	2453	266.805	26.407	0.644	2.053	0.913	-4.72904	137.3834	-4142.25
3	2453	165.684	24.916	0.592	2.943	0.908	-4.72904	137.3834	-4142.25
13	2459	308.921	20.88	0.755	1.108	0.935	-4.72908	137.3834	-4141.89
8	2466	158.76	21.789	0.562	2.349	0.873	-4.72987	137.3835	-4138.69
16	2468	240.477	25.219	0.733	2.077	0.956	-4.73003	137.3834	-4138.28
12	2473	185.088	21.69	0.681	1.996	0.931	-4.7301	137.3831	-4137.02
19	2473	217.678	20.983	0.77	1.589	0.946	-4.7301	137.3831	-4137.02
22	2473	174.063	22.257	0.664	2.235	0.922	-4.7301	137.3831	-4137.02
3	2475	257.853	21.815	0.771	1.45	0.912	-4.73021	137.3835	-4135.54
4	2475	740.66	34.211	0.816	1.241	0.956	-4.73021	137.3835	-4135.54
9	2475	271.7	26.044	0.68	1.961	0.913	-4.73021	137.3835	-4135.54
10	2475	382.965	25.802	0.814	1.365	0.954	-4.73021	137.3835	-4135.54
11	2475	442.544	31.391	0.712	1.749	0.949	-4.73021	137.3835	-4135.54
5	2476	265.217	24.761	0.677	1.816	0.929	-4.73023	137.3834	-4135.29
9	2476	229.585	23.774	0.677	1.933	0.919	-4.73023	137.3834	-4135.29
10	2476	280.432	21.676	0.829	1.316	0.956	-4.73023	137.3834	-4135.29
15	2476	529.421	32.366	0.623	1.554	0.895	-4.73023	137.3834	-4135.29
3	2477	278.58	24.545	0.682	1.699	0.898	-4.73027	137.3837	-4134.37
7	2477	131.771	20.892	0.603	2.602	0.886	-4.73027	137.3837	-4134.37
9	2477	563.422	30.718	0.824	1.315	0.965	-4.73027	137.3837	-4134.37

3	2480	236.552	22.78	0.709	1.723	0.947	-4.73041	137.3835	-4133.14
5	2480	149.94	20.624	0.691	2.228	0.937	-4.73041	137.3835	-4133.14
16	2480	303.408	29.784	0.655	2.296	0.906	-4.73041	137.3835	-4133.14
19	2480	177.326	28.228	0.457	3.529	0.91	-4.73041	137.3835	-4133.14
5	2481	495.112	27.401	0.728	1.191	0.924	-4.73031	137.3835	-4133.36
17	2555	202.243	23.73	0.616	2.187	0.93	-4.73091	137.3835	-4129.62
14	2556	315.183	23.94	0.705	1.428	0.894	-4.73093	137.3835	-4129.37
1	2565	209.299	21.383	0.731	1.716	0.942	-4.7318	137.3832	-4123.76
5	2565	498.596	30.159	0.756	1.433	0.947	-4.7318	137.3832	-4123.76
2	2568	231.129	21.497	0.823	1.57	0.967	-4.73237	137.3834	-4119.54
3	2568	710.1	32.125	0.822	1.141	0.962	-4.73237	137.3834	-4119.54
4	2568	372.161	24.609	0.847	1.278	0.962	-4.73237	137.3834	-4119.54
8	2568	173.005	20.252	0.745	1.862	0.95	-4.73237	137.3834	-4119.54
9	2568	261.514	26.858	0.697	2.166	0.952	-4.73237	137.3834	-4119.54
10	2568	1222.587	47.871	0.76	1.472	0.95	-4.73237	137.3834	-4119.54
17	2586	341.379	24.751	0.679	1.409	0.936	-4.7325	137.3824	-4121.5
28	2586	442.809	32.973	0.722	1.928	0.955	-4.7325	137.3824	-4121.5
33	2586	144.119	20.551	0.706	2.302	0.957	-4.7325	137.3824	-4121.5
27	2590	285.283	22.647	0.836	1.412	0.962	-4.73253	137.3822	-4124.29
28	2590	1031.545	41.992	0.777	1.343	0.953	-4.73253	137.3822	-4124.29
29	2590	275.14	24.188	0.738	1.67	0.952	-4.73253	137.3822	-4124.29
13	2593	255.781	21.13	0.728	1.371	0.925	-4.73295	137.3817	-4123.34
27	2593	306.628	23.525	0.814	1.418	0.956	-4.73295	137.3817	-4123.34

Bibliography

R. Anderson. Geologic mapping and characterization of gale crater and implications for its potential as a mars science laboratory landing site. *The Mars Journal*, 5, 9 2010. ISSN 15481921. doi: 10.1555/mars.2010.0004.

J.-P. Bibring, Y. Langevin, J. F. Mustard, F. Poulet, R. Arvidson, A. Gendrin, B. Gondet, N. Mangold, P. Pinet, F. Forget, M. Berthe, J.-P. Bibring, A. Gendrin, C. Gomez, B. Gondet, D. Jouglet, F. Poulet, A. Soufflot, M. Vincendon, M. Combes, P. Drossart, T. Encrenaz, T. Fouchet, R. Merchiorri, G. Belluci, F. Altieri, V. Formisano, F. Capaccioni, P. Cerroni, A. Coradini, S. Fonti, O. Korablev, V. Kottsov, N. Ignatiev, V. Moroz, D. Titov, L. Zasova, D. Loiseau, N. Mangold, P. Pinet, S. Doute, B. Schmitt, C. Sotin, E. Hauber, H. Hoffmann, R. Jaumann, U. Keller, R. Arvidson, J. F. Mustard, T. Duxbury, F. Forget, and G. Neukum. Global mineralogical and aqueous mars history derived from omega/mars express data. *Science*, 312, 4 2006. ISSN 0036-8075. doi: 10.1126/science.1122659.

N. T. Bridges, J. E. Laity, R. Greeley, J. Phoreman, and E. E. Eddlemon. Insights on rock abrasion and ventifact formation from laboratory and field analog studies with applications to mars. *Planetary and Space Science*, 52, 1 2004. ISSN 00320633. doi: 10.1016/j.pss.2003.08.026.

T. F. Bristow, E. B. Rampe, J. P. Grotzinger, V. K. Fox, K. A. Bennett, A. S. Yen, A. R. Vasavada, D. T. Vaniman, V. Tu, A. H. Treiman, M. T. Thorpe, S. M. Morrison, R. V. Morris, D. W. Ming, A. C. Mcadam, C. A. Malespin, P. R. Mahaffy, R. M. Hazen, S. Gupta, R. T. Downs, G. W. Downs, D. J. D. Marais, J. A. Crisp, P. I. Craig, S. J. Chipera, N. Castle, D. F. Blake, and C. N. Achilles. Clay minerals of glen torridon, mount sharp, gale crater, mars. *LPSC IX. 2089 (abstract)*, 2019.

A. B. Bryk, W. E. Dietrich, V. K. Fox, K. A. Bennett, S. G. Banham, M. P. Lamb, J. P. Grotzinger, A. R. Vasavada, K. M. Stack, R. Arvidson, C. M. Fedo, S. Gupta, R. C. Wiens, R. M. E. Williams, R. E. Kronyak, M. L. Turner, K. W. Lewis, D. M. Rubin, W. N. Rapin, L. L. Deit, S. L. Mouélic, K. S. Edgett, A. A. Fraeman, M. N. Hughes, L. C. Kah, and C. C. Bedford. The stratigraphy of central and western butte and the greenheugh pediment contact. *Lunar Planet. Sci. LI, 2612 (abstract).*, 2020.

A. Cailleux. L'indice d'emoussé des grains de sable et grés. *Rev. Geomorphol.*, Dyn 3:78–87, 1947.

A. Cousin, M. Desjardins, E. Dehouck, O. Forni, G. David, G. Berger, G. Caravaca, P. Meslin, J. Lasue, A. Ollila, W. Rapin, P. Gasda, S. Maurice, O. Gasnault, R. Wiens, and L. Beauvais. K-rich rubbly bedrock at glen torridon, gale crater, mars: Investigating the possible presence of illite. *Lunar Planet. Sci. LII, 2548 (abstract).*, 2021.

E. Dehouck, A. Cousin, N. Mangold, J. Frydenvang, J. Lasue, P.-Y. Meslin, O. Gasnault, V. Fox, K. Bennett, S. Maurice, and R. Wiens. Geochemistry of the clay-bearing sedimentary rocks of glen torridon, gale crater, mars. *EPSC*, 13, 2019.

L. L. Deit, E. Hauber, F. Fueten, M. Pondrelli, A. P. Rossi, and R. Jaumann. Sequence of infilling events in gale crater, mars: Results from morphology, stratigraphy, and mineralogy. *Journal of Geophysical Research: Planets*, 118, 12 2013. ISSN 21699097. doi: 10.1002/2012JE004322.

M. Durand and S. Bourquin. Criteria for the identification of ventifacts in the geological record: A review and new insights. *Comptes Rendus Geoscience*, 345, 3 2013. ISSN 16310713. doi: 10.1016/j.crte.2013.02.004.

L. A. Edgar, C. M. Fedo, S. Gupta, S. G. Banham, A. A. Fraeman, J. P. Grotzinger, K. M. Stack, N. T. Stein, K. A. Bennett, F. Rivera-Hernández, V. Sun, K. S. Edgett, D. M. Rubin, C. House, and J. V. Beek. A lacustrine paleoenvironment recorded at vera rubinridge, gale crater: Overview of the sedimentology and stratigraphy observed by the mars sciencelaboratory curiosity rover. *Journal of Geophysical Research: Planets*, 125, 3 2020. ISSN 2169-9097. doi: 10.1029/2019JE006307.

C. Fedo, J. Grotzinger, S. Gupta, N. T. Stein, J. Watkins, S. Banham, K. S. Edgett, M. Minitti, J. Schieber, K. Siebach, K. Stack-Morgan, H. Newsom, K. W. Lewis, C. House, and A. R. Vasavada. Facies analysis and basin architecture of the upper part of the murray formation, gale crater, mars. *Lunar Planet. Sci. XLVIII, 1689 (abstract).*, 2017.

V. K. Fox, K. A. Bennett, A. Bryk, R. Arvidson, T. Bristow, E. Dehouck, B. Dietrich, B. Ehlmann, C. Fedo, and N. Mangold. One year in glen torridon: Key results from the mars science laboratory curiosity rover exploration of clay-bearing units. *Lunar Planet. Sci. LI, 2833 (abstract).*, 2020.

A. A. Fraeman, B. L. Ehlmann, R. E. Arvidson, C. S. Edwards, J. P. Grotzinger, R. E. Milliken, D. P. Quinn, and M. S. Rice. The stratigraphy and evolution of lower mount sharp from spectral, morphological, and thermophysical orbital data sets. *Journal of Geophysical Research: Planets*, 121, 9 2016. ISSN 21699097. doi: 10.1002/2016JE005095.

A. A. Fraeman, L. A. Edgar, E. B. Rampe, L. M. Thompson, J. Frydenvang, C. M. Fedo, J. G. Catalano, W. E. Dietrich, T. S. J. Gabriel, A. R. Vasavada, J. P. Grotzinger, J. L'Haridon, N. Mangold, V. Z. Sun, C. H. House, A. B. Bryk, C. Hardgrove, S. Czarnecki, K. M. Stack, R. V. Morris, R. E. Arvidson, S. G. Banham,

K. A. Bennett, J. C. Bridges, C. S. Edwards, W. W. Fischer, V. K. Fox, S. Gupta, B. H. N. Horgan, S. R. Jacob, J. R. Johnson, S. S. Johnson, D. M. Rubin, M. R. Salvatore, S. P. Schwenzer, K. L. Siebach, N. T. Stein, S. M. R. Turner, D. F. Wellington, R. C. Wiens, A. J. Williams, G. David, and G. M. Wong. Evidence for a diagenetic origin of vera rubin ridge, gale crater, mars: Summary and synthesis of curiosity 's exploration campaign. *Journal of Geophysical Research: Planets*, 125, 12 2020. ISSN 2169-9097. doi: 10.1029/2020JE006527.

J. P. Grotzinger, D. Y. Sumner, L. C. Kah, K. Stack, S. Gupta, L. Edgar, D. Rubin, K. Lewis, J. Schieber, N. Mangold, R. Milliken, P. G. Conrad, D. DesMarais, J. Farmer, K. Siebach, F. Calef, J. Hurowitz, S. M. McLennan, D. Ming, D. Vaniman, J. Crisp, A. Vasavada, K. S. Edgett, M. Malin, D. Blake, R. Gellert, P. Mahaffy, R. C. Wiens, S. Maurice, J. A. Grant, S. Wilson, R. C. Anderson, L. Beegle, R. Arvidson, B. Hallet, R. S. Sletten, M. Rice, J. Bell, J. Griffes, B. Ehlmann, R. B. Anderson, T. F. Bristow, W. E. Dietrich, G. Dromart, J. Eigenbrode, A. Fraeman, C. Hardgrove, K. Herkenhoff, L. Jandura, G. Kocurek, S. Lee, L. A. Leshin, R. Leveille, D. Limonadi, J. Maki, S. McCloskey, M. Meyer, M. Minitti, H. Newsom, D. Oehler, A. Okon, M. Palucis, T. Parker, S. Rowland, M. Schmidt, S. Squyres, A. Steele, E. Stolper, R. Summons, A. Treiman, R. Williams, A. Yingst, M. S. Team, O. Kemppinen, N. Bridges, J. R. Johnson, D. Cremers, A. Godber, M. Wadhwa, D. Wellington, I. McEwan, C. Newman, M. Richardson, A. Charpentier, L. Peret, P. King, J. Blank, G. Weigle, S. Li, K. Robertson, V. Sun, M. Baker, C. Edwards, K. Farley, H. Miller, M. Newcombe, C. Pilorget, C. Brunet, V. Hipkin, R. Leveille, G. Marchand, P. S. Sanchez, L. Favot, G. Cody, L. Fluckiger, D. Lees, A. Nefian, M. Martin, M. Gailhanou, F. Westall, G. Israel, C. Agard, J. Baroukh, C. Donny, A. Gaboriaud, P. Guillemot, V. Lafaille, E. Lorigny, A. Paillet, R. Perez, M. Saccoccio, C. Yana, C. Armiens-Aparicio, J. C. Rodriguez, I. C. Blazquez, F. G. Gomez, J. Gomez-Elvira, S. Hettrich, A. L. Malvitte, M. M. Jimenez, J. Martinez-Frias, J. Martin-Soler, F. J. Martin-Torres, A. M. Jurado, L. Mora-Sotomayor, G. M. Caro, S. N. Lopez, V. Peinado-Gonzalez, J. Pla-Garcia, J. A. R. Manfredi, J. J. Romeral-Planello, S. A. S. Fuentes, E. S. Martinez, J. T. Redondo, R. Urqui-O'Callaghan, M.-P. Z. Mier, S. Chipera, J.-L. Lacour, P. Mauchien, J.-B. Sirven, H. Manning, A. Fairen, A. Hayes, J. Joseph, R. Sullivan, P. Thomas, A. Dupont, A. Lundberg, N. Melikechi, A. Mezzacappa, J. DeMarines, D. Grinspoon, G. Reitz, B. Prats, E. Atlaskin, M. Genzer, A.-M. Harri, H. Haukka, H. Kahanpaa, J. Kauhanen, M. Paton, J. Polkko, W. Schmidt, T. Siili, C. Fabre, J. Wray, M. B. Wilhelm, F. Poitrasson, K. Patel, S. Gorevan, S. Indyk, G. Paulsen, D. Bish, B. Gondet, Y. Langevin, C. Geffroy, D. Baratoux, G. Berger, A. Cros, C. d'Uston, O. Forni, O. Gasnault, J. Lasue, Q.-M. Lee, P.-Y. Meslin, E. Pallier, Y. Parot, P. Pinet, S. Schroder, M. Toplis, E. Lewin, W. Brunner, E. Heydari, C. Achilles, B. Sutter, M. Cabane, D. Coscia, C. Szopa, F. Robert, V. Sautter, S. L. Mouelic, M. Nachon, A. Buch, F. Stalport, P. Coll, P. Francois, F. Raulin, S. Teinturier, J. Cameron, S. Clegg, A. Cousin, D. DeLapp, R. Dingler, R. S. Jackson, S. Johnstone, N. Lanza, C. Little, T. Nelson, R. B. Williams, A. Jones, L. Kirkland, B. Baker, B. Cantor, M. Caplinger, S. Davis, B. Duston, D. Fay, D. Harker, P. Her-

rera, E. Jensen, M. R. Kennedy, G. Krezoski, D. Krysak, L. Lipkaman, E. McCartney, S. McNair, B. Nixon, L. Posiolova, M. Ravine, A. Salamon, L. Saper, K. Stoiber, K. Supulver, J. V. Beek, T. V. Beek, R. Zimdar, K. L. French, K. Iagnemma, K. Miller, F. Goesmann, W. Goetz, S. Hviid, M. Johnson, M. Lefavor, E. Lyness, E. Breves, M. D. Dyar, C. Fassett, L. Edwards, R. Haberle, T. Hoehler, J. Hollingsworth, M. Kahre, L. Keely, C. McKay, L. Bleacher, W. Brinckerhoff, D. Choi, J. P. Dworkin, M. Floyd, C. Freissinet, J. Garvin, D. Glavin, D. Harpold, D. K. Martin, A. McAdam, A. Pavlov, E. Raaen, M. D. Smith, J. Stern, F. Tan, M. Trainer, A. Posner, M. Voytek, A. Aubrey, A. Behar, D. Blaney, D. Brinza, L. Christensen, L. DeFlores, J. Feldman, S. Feldman, G. Flesch, I. Jun, D. Keymeulen, M. Mischna, J. M. Morookian, B. Pavri, M. Schoppers, A. Sengstacken, J. J. Simmonds, N. Spanovich, M. d. l. T. Juarez, C. R. Webster, A. Yen, P. D. Archer, F. Cucinotta, J. H. Jones, R. V. Morris, P. Niles, E. Rampe, T. Nolan, M. Fisk, L. Radziemski, B. Barraclough, S. Bender, D. Berman, E. N. Dobrea, R. Tokar, T. Cleghorn, W. Huntress, G. Manhes, J. Hudgins, T. Olson, N. Stewart, P. Sarrazin, E. Vicenzi, M. Bullock, B. Ehresmann, V. Hamilton, D. Hassler, J. Peterson, S. Rafkin, C. Zeitlin, F. Fedosov, D. Golovin, N. Karpushkina, A. Kozyrev, M. Litvak, A. Malakhov, I. Mitrofanov, M. Mokrousov, S. Nikiforov, V. Prokhorov, A. Sanin, V. Tretyakov, A. Varenikov, A. Vostrukhin, R. Kuzmin, B. Clark, M. Wolff, O. Botta, D. Drake, K. Bean, M. Lemmon, S. P. Schwenzer, E. M. Lee, R. Sucharski, M. A. d. P. Hernandez, J. J. B. Avalos, M. Ramos, M.-H. Kim, C. Malespin, I. Plante, J.-P. Muller, R. Navarro-Gonzalez, R. Ewing, W. Boynton, R. Downs, M. Fitzgibbon, K. Harshman, S. Morrison, O. Kortmann, A. Williams, G. Lugmair, M. A. Wilson, B. Jakosky, T. Balic-Zunic, J. Frydenvang, J. K. Jensen, K. Kinch, A. Koefoed, M. B. Madsen, S. L. S. Stipp, N. Boyd, J. L. Campbell, G. Perrett, I. Pradler, S. VanBommel, S. Jacob, T. Owen, H. Savijarvi, E. Boehm, S. Bottcher, S. Burmeister, J. Guo, J. Kohler, C. M. Garcia, R. Mueller-Mellin, R. Wimmer-Schweingruber, J. C. Bridges, T. McConnochie, M. Benna, H. Franz, H. Bower, A. Brunner, H. Blau, T. Boucher, M. Carmosino, S. Atreya, H. Elliott, D. Halleaux, N. Renno, M. Wong, R. Pepin, B. Elliott, J. Spray, L. Thompson, S. Gordon, A. Ollila, J. Williams, P. Vasconcelos, J. Bentz, K. Nealson, R. Popa, J. Moersch, C. Tate, M. Day, R. Francis, E. McCullough, E. Cloutis, I. L. ten Kate, D. Scholes, S. Slavney, T. Stein, J. Ward, J. Berger, and J. E. Moores. A habitable fluvio-lacustrine environment at yellowknife bay, gale crater, mars. *Science*, 343, 1 2014. ISSN 0036-8075. doi: 10.1126/science.1242777.

J. P. Grotzinger, S. Gupta, M. C. Malin, D. M. Rubin, J. Schieber, K. Siebach, D. Y. Sumner, K. M. Stack, A. R. Vasavada, R. E. Arvidson, F. Calef, L. Edgar, W. F. Fischer, J. A. Grant, J. Griffes, L. C. Kah, M. P. Lamb, K. W. Lewis, N. Mangold, M. E. Minitti, M. Palucis, M. Rice, R. M. Williams, R. A. Yingst, D. Blake, D. Blaney, P. Conrad, J. Crisp, W. E. Dietrich, G. Dromart, K. S. Edgett, R. C. Ewing, R. Gellert, J. A. Hurowitz, G. Kocurek, P. Mahaffy, M. J. McBride, S. M. McLennan, M. Mischna, D. Ming, R. Milliken, H. Newsom, D. Oehler, T. J. Parker, D. Vaniman, R. C. Wiens, and S. A. Wilson. Deposition, exhumation, and paleoclimate of an ancient lake deposit, gale crater, mars. *Science*, 350, 10 2015.

ISSN 10959203. doi: 10.1126/science.aac7575.

C. H. Hugenholtz, T. E. Barchyn, and E. A. Favaro. Formation of periodic bedrock ridges on earth. *Aeolian Research*, 18, 9 2015. ISSN 18759637. doi: 10.1016/j.aeolia.2015.07.002.

J. B. III, A. Godber, M. Rice, A. Fraeman, B. Ehlmann, W. Goetz, C. Hardgrove, D. Harker, J. Johnson, K. Kinch, M. Lem-mon, S. McNair, S. L. Mouélic, M. Madsen, M. Malin, and the MSL Science Team. Initial multispectral imaging results from the mars science laboratory mastcam investigation at the gale crater field site. *Lunar Planet. Sci. XLIV, 1417 (abstract)*, 2013.

M. Malin, M. Caplinger, K. Edgett, F. Ghaemi, M. Ravine, J. Schaffner, J. Baker, J. Bardis, D. Dibiase, J. Maki, R. Willson, J. Bell, W. Dietrich, L. Edwards, B. Hallet, K. Herkenhoff, E. Heydari, L. Kah, M. Lemmon, and M. Minitti. The mars science laboratory (msl) mast-mounted cameras (mastcams) flight instruments. *Lunar Planet. Sci. XLI, 1123 (abstract)*, 2010.

M. C. Malin, M. A. Caplinger, K. S. Edgett, F. T. Ghaemi, M. A. Ravine, J. A. Schaffner, J. N. Maki, R. G. Willson, J. F. B. Iii, J. F. Cameron, W. E. Dietrich, L. J. Edwards, B. Hallet, K. E. Herken-Hoff, E. Heydari, L. C. Kah, M. T. Lemmon, M. E. Minitti, T. S. Olson, T. J. Parker, S. K. Rowland, J. Schieber, R. J. Sullivan, D. Y. Sumner, P. C. Thomas, and R. A. Yingst. The mars science laboratory (msl) mars descent imager (mardi) flight instrument. *Lunar Planet. Sci. XL, 1199 (abstract)*, 2009. URL `http://www.msss.com/msl/mardi/prelaunch`$_i$*mages/*.

M. C. Malin, M. A. Ravine, M. A. Caplinger, F. T. Ghaemi, J. A. Schaffner, J. N. Maki, J. F. Bell, J. F. Cameron, W. E. Dietrich, K. S. Edgett, L. J. Edwards, J. B. Garvin, B. Hallet, K. E. Herkenhoff, E. Heydari, L. C. Kah, M. T. Lemmon, M. E. Minitti, T. S. Olson, T. J. Parker, S. K. Rowland, J. Schieber, R. Sletten, R. J. Sullivan, D. Y. Sumner, R. A. Yingst, B. M. Duston, S. McNair, and E. H. Jensen. The mars science laboratory (msl) mast cameras and descent imager: Investigation and instrument descriptions. *Earth and Space Science*, 4, 8 2017. ISSN 23335084. doi: 10.1002/2016EA000252.

S. Maurice, R. C. Wiens, M. Saccoccio, B. Barraclough, O. Gasnault, O. Forni, N. Mangold, D. Baratoux, S. Bender, G. Berger, J. Bernardin, M. Berthé, N. Bridges, D. Blaney, M. Bouyé, P. Caïs, B. Clark, S. Clegg, A. Cousin, D. Cremers, A. Cros, L. DeFlores, C. Derycke, B. Dingler, G. Dromart, B. Dubois, M. Dupieux, E. Durand, L. d'Uston, C. Fabre, B. Faure, A. Gaboriaud, T. Gharsa, K. Herkenhoff, E. Kan, L. Kirkland, D. Kouach, J.-L. Lacour, Y. Langevin, J. Lasue, S. L. Mouélic, M. Lescure, E. Lewin, D. Limonadi, G. Manhès, P. Mauchien, C. McKay, P.-Y. Meslin, Y. Michel, E. Miller, H. E. Newsom, G. Orttner, A. Paillet, L. Parès, Y. Parot, R. Pérez, P. Pinet, F. Poitrasson, B. Quertier, B. Sallé, C. Sotin, V. Sautter, H. Séran, J. J. Simmonds, J.-B. Sirven, R. Stiglich, N. Striebig, J.-J. Thocaven, M. J. Toplis, and D. Vaniman. The chemcam instrument suite on the mars science laboratory (msl) rover: Science objectives and mast unit description.

Space Science Reviews, 170, 9 2012. ISSN 0038-6308. doi: 10.1007/s11214-012-9912-2.

R. E. Milliken, G. A. Swayze, B. J. Thomson, K. S. Edgett, G. Swayze, R. N. Clark, B. J. Thomson, R. Anderson, and J. F. B. III. Clay and sulfate-bearing rocks in a stratigraphic sequence in gale crater. *Lunar Planet. Sci. XL, 1479 (abstract).*, 2009. URL `https://www.researchgate.net/publication/253083302`.

R. E. Milliken, J. P. Grotzinger, and B. J. Thomson. Paleoclimate of mars as captured by the stratigraphic record in gale crater. *Geophysical Research Letters*, 37, 2 2010. ISSN 00948276. doi: 10.1029/2009GL041870.

R. E. Milliken, R. C. Ewing, W. W. Fischer, and J. Hurowitz. Wind-blown sandstones cemented by sulfate and clay minerals in gale crater, mars. *Geophysical Research Letters*, 41, 2 2014. ISSN 00948276. doi: 10.1002/2013GL059097.

M. E. Minitti, M. C. Malin, J. K. V. Beek, M. Caplinger, J. N. Maki, M. Ravine, F. J. Calef, L. A. Edgar, D. Harker, K. E. Herkenhoff, L. C. Kah, M. R. Kennedy, G. M. Krezoski, R. E. Kronyak, L. Lipkaman, B. Nixon, S. K. Rowland, J. Schieber, J. F. Schroeder, K. M. Stack, R. M. Williams, and R. A. Yingst. Distribution of primary and secondary features in the pahrump hills outcrop (gale crater, mars) as seen in a mars descent imager (mardi) "sidewalk" mosaic. *Icarus*, 328, 8 2019. ISSN 00191035. doi: 10.1016/j.icarus.2019.03.005.

D. Nurfiani and C. B. de Maisonneuve. Furthering the investigation of eruption styles through quantitative shape analyses of volcanic ash particles. *Journal of Volcanology and Geothermal Research*, 354, 4 2018. ISSN 03770273. doi: 10.1016/j.jvolgeores.2017.12.001.

C. D. O'Connell-Cooper, L. M. Thompson, R. Gellert, J. G. Spray, N. I. Boyd, J. Berger, M. Mccraig, S. J. Vanbommel, and A. Yen. Apxs geochemistry of the fractured intermediate unit (fiu)-its relationship to underlying glen torridon units and overlying pediment rocks at the greenheugh unconformity. *Lunar Planet. Sci. LII, 2405 (abstract).*, 2021.

J. D. Pelletier, A. L. Leier, and J. R. Steidtmann. Wind-driven reorganization of coarse clasts on the surface of mars. *Geology*, 37, 1 2009. ISSN 1943-2682. doi: 10.1130/G25071A.1.

M. C. Powers. A new roundness scale for sedimentary particles. *SEPM Journal of Sedimentary Research*, Vol. 23, 1953. ISSN 1527-1404. doi: 10.1306/D4269567-2B26-11D7-8648000102C1865D.

N. A. Riley. Projection sphericity. *SEPM Journal of Sedimentary Research*, Vol. 11, 1941. ISSN 1527-1404. doi: 10.1306/D426910C-2B26-11D7-8648000102C1865D.

F. Rivera-Hernández, D. Y. Sumner, N. Mangold, K. M. Stack, O. Forni, H. Newsom, A. Williams, M. Nachon, J. L'Haridon, O. Gasnault, R. Wiens, and S. Maurice.

Using chemcam libs data to constrain grain size in rocks on mars: Proof of concept and application to rocks at yellowknife bay and pahrump hills, gale crater. *Icarus*, 321, 3 2019. ISSN 00191035. doi: 10.1016/j.icarus.2018.10.023.

V. Sautter, C. Fabre, O. Forni, M. J. Toplis, A. Cousin, A. M. Ollila, P. Y. Meslin, S. Maurice, R. C. Wiens, D. Baratoux, N. Mangold, S. L. Mouélic, O. Gasnault, G. Berger, J. Lasue, R. A. Anderson, E. Lewin, M. Schmidt, D. Dyar, B. L. Ehlmann, J. Bridges, B. Clark, and P. Pinet. Igneous mineralogy at bradbury rise: The first chemcam campaign at gale crater. *Journal of Geophysical Research: Planets*, 119, 1 2014. ISSN 21699097. doi: 10.1002/2013JE004472.

V. Sautter, M. J. Toplis, R. C. Wiens, A. Cousin, C. Fabre, O. Gasnault, S. Maurice, O. Forni, J. Lasue, A. Ollila, J. C. Bridges, N. Mangold, S. L. Mouélic, M. Fisk, P.-Y. Meslin, P. Beck, P. Pinet, L. L. Deit, W. Rapin, E. M. Stolper, H. Newsom, D. Dyar, N. Lanza, D. Vaniman, S. Clegg, and J. J. Wray. In situ evidence for continental crust on early mars. *Nature Geoscience*, 8, 8 2015. ISSN 1752-0894. doi: 10.1038/ngeo2474.

K. M. Stack, J. P. Grotzinger, M. P. Lamb, S. Gupta, D. M. Rubin, L. C. Kah, L. A. Edgar, D. M. Fey, J. A. Hurowitz, M. McBride, F. Rivera-Hernández, D. Y. Sumner, J. K. V. Beek, R. M. Williams, and R. A. Yingst. Evidence for plunging river plume deposits in the pahrump hills member of the murray formation, gale crater, mars. *Sedimentology*, 66:1768–1802, 8 2019a. ISSN 13653091. doi: 10.1111/sed.12558.

K. M. Stack, V. Z. Sun, R. E. Arvidson, C. Fedo, M. Day, K. Bennett, L. A. Edgar, V. K. Fox, and S. Cofield. Origin of linear ridges in the clay-bearing unit of mount sharp, gale crater, mars. *Lunar Planet. Sci. L, 1210 (abstract).*, 2019b.

B. Thomson, N. Bridges, R. Milliken, A. Baldridge, S. Hook, J. Crowley, G. Marion, C. de Souza Filho, A. Brown, and C. Weitz. Constraints on the origin and evolution of the layered mound in gale crater, mars using mars reconnaissance orbiter data. *Icarus*, 214, 8 2011. ISSN 00191035. doi: 10.1016/j.icarus.2011.05.002.

K. X. Whipple and T. Dunne. The influence of debris-flow rheology on fan morphology, owens valley, california. *GSA Bulletin*, 104:887–900, 7 1992. ISSN 0016-7606. doi: 10.1130/0016-7606(1992)104<0887:TIODFR>2.3.CO;2. URL `https://doi.org/10.1130/0016-7606(1992)104<0887:TIODFR>2.3.CO 2`.

R. A. Yingst, L. Crumpler, W. H. Farrand, R. Li, and P. D. Souza. Constraints on the geologic history of "home plate" materials provided by clast morphology and texture. *Journal of Geophysical Research E: Planets*, 115, 2010. ISSN 01480227. doi: 10.1029/2010JE003668.

R. A. Yingst, L. C. Kah, M. Palucis, R. M. Williams, J. Garvin, J. C. Bridges, N. Bridges, R. G. Deen, J. Farmer, O. Gasnault, W. Goetz, V. E. Hamilton, V. Hipkin, J. K. Jensen, P. L. King, A. Koefoed, S. P. L. Mouélic, M. B. Madsen, N. Mangold, J. Martinez-Frias, S. Maurice, E. M. McCartney, H. Newsom, O. Pariser,

V. H. Sautter, and R. C. Wiens. Characteristics of pebble- and cobble-sized clasts along the curiosity rover traverse from bradbury landing to rocknest. *Journal of Geophysical Research E: Planets*, 118:2361–2380, 11 2013. ISSN 01480227. doi: 10.1002/2013JE004435.

R. A. Yingst, K. Cropper, S. Gupta, L. C. Kah, R. M. Williams, J. Blank, F. Calef, V. E. Hamilton, K. Lewis, J. Shechet, M. McBride, N. Bridges, J. M. Frias, and H. Newsom. Characteristics of pebble and cobble-sized clasts along the curiosity rover traverse from sol 100 to 750: Terrain types, potential sources, and transport mechanisms. *Icarus*, 280:72–92, 12 2016. ISSN 10902643. doi: 10.1016/j.icarus.2016.03.001.